*Mon. Not. R. astr. Soc.* (1988) **232,** 431–461

# Analysis of a complete galaxy redshift survey – II. The field-galaxy luminosity function

G. Efstathiou *Institute of Astronomy, Madingley Road, Cambridge CB3 0HA*

Richard S. Ellis *Physics Department, University of Durham, Science Laboratories, South Road, Durham DH1 3LE*

Bruce A. Peterson *Mt Stromlo and Siding Spring Observatories, The Australian National University, Woden ACT 2606, Australia*

Accepted 1987 November 25. Received 1987 September 14

**Summary.** We present a detailed analysis of the field-galaxy luminosity function for five magnitude-limited redshift surveys. We apply maximum-likelihood estimators which we demonstrate provide unbiased estimates of the luminosity function for spatially inhomogeneous distributions under the assumption that luminosity is uncorrelated with position. A likelihood-ratio test is devised which can be used to assess whether specific functional forms of the luminosity function provide acceptable fits to the observations. These methods, and asymptotic estimates of their errors, are checked against Monte Carlo simulations. Our results show that the luminosity functions from the AARS, KOS and KOSS redshift surveys are all compatible with Schechter functions. The luminosity function for the CfA survey does not fit a Schechter function. In particular, the bright end falls off less steeply than a Schechter function, but we argue that this is caused by the large random errors in the Zwicky magnitudes. From these field surveys there is no evidence for morphological type differences in the field luminosity function for types earlier than Sc. Later type galaxies (Sc-I) are significantly fainter than earlier types. With the exception of the CfA survey, the luminosity functions derived from the redshift surveys are compatible with each other. We conclude that the field luminosity function is well described by a Schechter function with parameters $\alpha=-1.07\pm0.05$, $M^*_{B_T}=-19.68\pm0.10$, and $\phi^*=(1.56\pm0.34)\times10^{-2}\,\mathrm{Mpc}^{-3}$ for $H_0=100\,\mathrm{km\,s^{-1}\,Mpc^{-1}}$.

## 1 Introduction

The galaxy luminosity function and any dependence it may have on environment and morphological type is of fundamental importance in cosmology. In this paper we investigate the luminosity function of field galaxies.

The optical galaxy luminosity function has been the subject of numerous investigations [see the reviews by Felten (1977, 1985) and references therein]. A knowledge of the luminosity function is essential in interpreting galaxy number counts (e.g. Ellis, 1983, 1987), statistics of galaxy clustering based on magnitude-limited catalogues (e.g. Groth & Peebles 1977) and in analysing the spatial distribution of galaxies from redshift surveys (e.g. Kirshner, Oemler & Schechter 1978, 1979, hereafter KOS; Davis & Peebles 1983a). In addition, the shape of the galaxy luminosity function is of theoretical interest as it may provide constraints on models of galaxy formation (White & Rees 1978; Frenk *et al.* 1988).

Several years ago, we completed a redshift survey [the Anglo–Australian Redshift Survey, hereafter AARS, Peterson *et al.* (1986), Paper III] to investigate various aspects of galaxy clustering (Bean *et al.* 1983, Paper I; Shanks *et al.* 1984a). A secondary aim was to provide a determination of the field luminosity function. The AARS is deep enough that systematic errors in the luminosity function caused by the density enhancement and the peculiar velocity field associated with the Local Supercluster are expected to be negligible. Furthermore, the AARS was constructed using a photometric system similar to that used in most of the studies of deep number counts (e.g. Peterson *et al.* 1979; Shanks *et al.* 1984b). In order to improve on the techniques commonly used to determine luminosity functions, we devised a maximum-likelihood method to provide an unbiased estimate of the luminosity function, together with reliable error estimates, which would be unaffected by spatial inhomogeneities, i.e. clustering. In addition, we developed a statistic for assessing whether a simple parametric formula, e.g. the Schechter (1976) function, provides an acceptable fit to the data. These methods are described in Section 2 and are checked in detail against Monte Carlo simulations. The techniques should prove useful in analysing other redshift surveys (e.g. the *IRAS* sample – Lawrence *et al.* 1986) particularly if one has no preconceived notion that the results will be well fitted by, say, a Schechter function.

We also critically examine the field luminosity functions determined from four other redshift surveys. Published work is unsatisfactory in several respects. The early results reviewed by Felten (1977) are systematically biased by the density enhancement of the Local Supercluster. Sandage, Tammann & Yahil (1979, hereafter STY) and Tammann, Yahil & Sandage (1979) developed a maximum-likelihood technique which is not affected by such a bias. They applied it to estimate the luminosity function of the Revised Shapley–Ames Sample (hereafter RSA, Sandage & Tammann 1981). However, they did not include a model for the mean peculiar velocity field around the Local Supercluster (hereafter 'Virgo-infall') and hence their solutions are likely to be in error. Similarly, the analysis by KOS of a sample drawn from the *Second Reference Catalogue of Bright Galaxies* (RC2, de Vaucouleurs, de Vaucouleurs & Corwin 1976) also ignored Virgo-infall. Kraan-Korteweg, Sandage & Tammann (1984) re-analysed the RSA sample including Virgo-infall but used a method which did not account for biases caused by density inhomogeneities. Kirshner *et al.* (1983, hereafter KOSS) constructed a deep redshift survey similar to the AARS. Their analysis of the luminosity function gave results which apparently differed significantly from those of their earlier KOS survey and with their analysis of the RC2. Davis, Huchra & Latham (1983) found that the luminosity function of the Center for Astrophysics (CfA) redshift survey (Huchra *et al.* 1983) differed from the Schechter form, a result apparently at variance with those from other surveys. To check these points, we extended our original goal and made a complete analysis of the field luminosity function for all of the redshift surveys described above.

Felten (1985) has pointed out the difficulties in estimating luminosity functions and has drawn attention to some of the discrepancies in the literature. We address his points in detail in this paper. In Sections 3 and 4 we show that there are no serious differences in the shapes of the luminosity functions derived from these surveys, though there may be systematic discrepancies in the normalization. We have also analysed the luminosity functions for different morphological

types. Our main conclusions are summarized in Section 5. Throughout this paper we assume a Hubble constant of $H_0=100\,\mathrm{km\,s^{-1}\,Mpc^{-1}}$.

## 2 Methods

### 2.1 ESTIMATORS

The 'traditional' method (e.g. Felten 1977) of determining the luminosity function $\phi$ from a magnitude-limited sample is based on the estimator

$$dN(L)=\phi V(L, m_{\mathrm{lim}})\, dL, \tag{2.1}$$

where $dN(L)$ is the observed number of galaxies with luminosity in the range $(L-dL/2, L+dL/2)$ and $V(L, m_{\mathrm{lim}})$ is the total volume of space in which galaxies of luminosity $L$ can be seen in a catalogue of magnitude limit $m_{\mathrm{lim}}$. In shallow catalogues, such as the RSA and CfA surveys, the Local Supercluster represents a significant local density enhancement. The estimator (2.1) will then overestimate the contribution of intrinsically faint galaxies relative to luminous ones and will lead to a biased estimate of $\phi(L)$. Furthermore, any velocity field around the Virgo cluster will significantly distort the apparent spatial distribution of nearby galaxies if redshift is used to infer distance. One way of minimizing these problems is to use a deep catalogue, such that the depth is larger than the scale of any local inhomogeneity. The traditional estimator would then yield an unbiased determination of $\phi(L)$ over a wide range of luminosities. However, the deep surveys constructed so far have gained depth at the expense of solid angle. The distribution of galaxies with redshift $dN(z)$ thus shows marked fluctuations because galaxies are strongly clustered. This is illustrated in Fig. 1 which shows the $dN(z)$ distributions for the AAT and KOSS surveys. Applying equation (2.1) to such a sample would yield an estimate of the luminosity which is subject to large fluctuations, though the estimate would be correct in the mean. One way of reducing these fluctuations would be to adopt a random sampling strategy, as suggested by Kaiser (1986), in which one measures redshifts for only one in $\gtrsim$20 galaxies from a magnitude-limited catalogue.

Another method of reducing such errors is based on the assumption that the luminosity

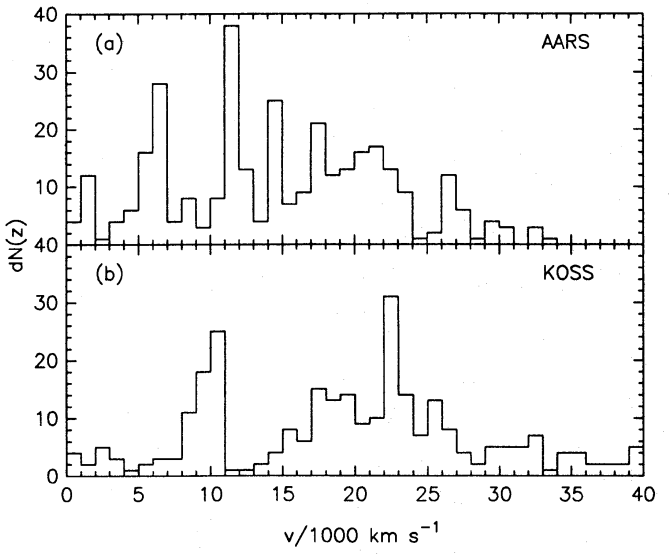


**Figure 1.** Redshift distribution of galaxies with $B_J<17.5$ in the AARS (Fig. 1a) and galaxies with $F_{\mathrm{KOS}}<17.0$ in the KOSS survey (Fig. 1b).

function has a universal form. Let the number of galaxies with luminosity in the interval $(L-dL/2, L+dL/2)$ in a volume element $d^3\mathbf{x}$ at position $\mathbf{x}$ be

$$p(L, \mathbf{x})\, dL\, d^3\mathbf{x} \tag{2.2}$$

and assume that $p(L, \mathbf{x})$ is separable,

$$p(L, \mathbf{x}) = \phi(L)\varrho(\mathbf{x}). \tag{2.3}$$

A number of estimators may then be devised in which the spatially dependent part $\varrho(\mathbf{x})$ factors out (Turner 1979; KOS; STY; Davis & Huchra 1982). These are reviewed below. Sandage, Binggeli & Tammann (1985) have analysed the luminosity functions for galaxies in the Virgo cluster and have shown convincingly that the luminosity function depends on morphological type, particularly at faint absolute magnitudes. Dressler (1980) has demonstrated that the mix of morphological types is closely related to local environment. Thus, the assumption (2.3) is certainly false in detail. However, the field surveys can only yield useful results within a range of absolute magnitudes $-22 \leqslant M_B \leqslant -16$ and we will show that morphological type dependences over this range (and for the pass-bands used in the surveys) are relatively small. Thus, we expect equation (2.3) to be a useful first approximation.

### 2.1.1 *Methods of Turner, KOS and Davis & Huchra*

If $N[>L, r \leqslant r_{\max}(L)]$ denotes the total number of galaxies brighter than $L$ with distance less than the maximum distance $r_{\max}(L)$ out to which a galaxy of luminosity $L$ could be observed in a magnitude-limited sample, then

$$\frac{dN(L)}{N[>L, r \leqslant r_{\max}(L)]} = \frac{\phi(L)\, dL}{\int_L^\infty \phi(L')\, dL'} = d \ln \Phi(L), \tag{2.4}$$

where $\Phi(L)$ is the integral luminosity function. This is the estimator adopted by KOS and Turner (1979). The method has the following disadvantages: (i) in estimating the shape of $\phi(L)$, information relating to faint galaxies at $<L$ is not used; (ii) the estimates of $d \ln \Phi(L)$ are not independent, thus the errors are correlated and difficult to estimate; (iii) it is not clear how best to apply the estimator in practice. For example, KOS assumed a Schechter function for $\phi(L)$ and then determined $L^*$ and $\alpha$ by a least-squares fit to the integral function. In tests of this method, we found the results to be sensitive to the sizes of the bin widths. Davis & Huchra (1982) use a variant of equation (2.4) in which the data are binned in equal distance intervals rather than in equal magnitude intervals. This somewhat reduces the problems caused by binning the data although the method still suffers from the other problems mentioned above.

### 2.1.2 *STY maximum likelihood method*

The probability that a galaxy with redshift $z_i$ and luminosity $L_i$ is seen in a magnitude-limited catalogue is

$$p_i \propto \phi(L_i) \Big/ \int_{L_{\min}(z_i)}^\infty \phi(L)\, dL. \tag{2.5}$$

Thus, we can define a likelihood function

$$\mathfrak{L} = \prod_i p_i, \tag{2.6}$$

and adopt a parametric model for $\phi(L)$ such as the Schechter function. The free parameters are determined by maximizing the likelihood function (2.6). The method has the following attractive features:

(i) The maximum likelihood method has well-defined asymptotic error properties (e.g. Kendall & Stuart 1961);

(ii) there is no requirement to select bin widths;

(iii) it is easy to use in multi-field surveys in which the completeness limit varies from field to field and it is straightforward to apply $K$-corrections to each object or groups of objects;

(iv) it is only weakly biased (see Section 2.2).

Thus, we have adopted this method in this paper. It has the disadvantage that it is difficult to test whether the assumed parametric form for $\phi(L)$ is a good fit to the data.

A simple and accurate method of estimating errors is to determine the ellipsoid of parameter values defined by

$$\ln \mathfrak{L} = \ln \mathfrak{L}_{\max} - \tfrac{1}{2}\chi^2_\beta(M), \tag{2.7}$$

where $\chi^2_\beta(M)$ is the $\beta$-point of the $\chi^2$ distribution with $M$ degrees of freedom. (An alternative method is to estimate the components of the information matrix as discussed in Appendix A.)

### *2.1.3 Stepwise maximum-likelihood method*

In this section, we develop a maximum-likelihood technique which does not rely on the assumption of a simple functional form for $\phi(L)$. Let us parameterize the luminosity function as $N_p$ steps:

$$\phi(L)=\phi_k, \qquad L_k-\Delta L/2<L<L_k+\Delta L/2, \qquad k=1,\ldots,N_p. \tag{2.8}$$

As in expressions (2.5) and (2.6), the likelihood is

$$\ln \mathfrak{L} = \sum_{i=1}^{N} W(L_i-L_k) \ln \phi_k - \sum_{i=1}^{N} \ln \left\{ \sum_{j=1}^{N_p} \phi_j \Delta L H[L_j - L_{\min}(z_i)] \right\} + \text{const}, \tag{2.9}$$

where $N$ is the total number of galaxies in the sample and

$$W(x)=\begin{cases} 1, & -\Delta L/2 \leqslant x \leqslant \Delta L/2; \\ 0, & \text{otherwise.} \end{cases} \tag{2.10a}$$

$$H(x)=\begin{cases} 0, & x \leqslant -\Delta L/2 \\ (x/\Delta L+1/2), & -\Delta L/2 \leqslant x \leqslant \Delta L/2 \\ 1, & x \geqslant \Delta L/2. \end{cases} \tag{2.10b}$$

Now, since the likelihood function involves ratios of the $\phi_k$, some sort of constraint must be imposed to fix the otherwise arbitrary normalization constant. A constraint is essential if the results from different samples are to be directly compared. We adopt a constraint of the form

$$g=\sum_k \phi_k (L_k/L_f)^\beta \Delta L - 1 = 0, \tag{2.11}$$

where $L_f$ is a fiducial luminosity and $\beta$ is a constant. The constraint is introduced into the likelihood equation using a Lagrangian multiplier $\lambda$, thus we maximize $\ln \mathfrak{L}' = \ln \mathfrak{L} + \lambda g(\phi_k)$ with respect to the $\phi_k$ and $\lambda$.

The likelihood equation then yields

$$\phi_k \Delta L = \frac{\sum_i W(L_i - L_k)}{\sum_i \left\{ H[L_k - L_{\min}(z_i)] \Big/ \sum_{j=1}^{N_p} \phi_j \Delta L H[L_j - L_{\min}(z_i)] \right\}}, \tag{2.12}$$

together with condition (2.11) and the requirement that $\lambda=0$. The constraint therefore does not affect the shape of the maximum likelihood estimate of $\phi$ but it does play a role in the error estimates. The constant $\beta$ may be chosen to give 'minimum variance' in a way which will be made precise in Section 2.2 below. The parameters $\phi_k$ may be rapidly determined from equation (2.12) by iteration.

To estimate errors we use the property that the maximum-likelihood estimates $\phi_k$ are asymptotically normally distributed with covariance matrix

$$\text{cov}\,(\phi_k) = \mathbf{I}^{-1}(\phi_k), \tag{2.13a}$$

where $\mathbf{I}(\phi_k)$ is the information matrix given by

$$\mathbf{I}(\phi_k) = -\begin{bmatrix} \partial^2 \ln \mathfrak{L} / \partial\phi_i \partial\phi_j + (\partial g/\partial\phi_i)(\partial g/\partial\phi_j) & \partial g/\partial\phi_j \\ \partial g/\partial\phi_i & 0 \end{bmatrix}_{\phi=\phi_k}. \tag{2.13b}$$

(see Eadie *et al.* 1971). Notice the inclusion of the term $(\partial g/\partial\phi_i)(\partial g/\partial\phi_j)$ which renders the information matrix non-singular. The convergence of the covariance matrix to the asymptotic expression (2.13) is considered in Section 2.2.

The estimator (2.12) is a generalization of the C-method of Lynden-Bell (1971; see also Jackson 1974) and is related to a method recently discussed by Choloniewski (1986). The method clearly has the advantage that no specific functional form is assumed. However, this feature is also at the heart of the method's major weakness – in most astrophysical applications we would expect the 'true' luminosity function to be smooth, but the method as described makes no use of any continuity assumptions. These could in principle be applied in the form of additional constraints, but these will not be considered in this paper. The method can easily be adapted to estimating multivariate functions, e.g. the joint optical–infrared luminosity function.

As an example of the method, consider the case when all galaxies are at the same redshifts $z_s$ and we apply the constraint

$$\sum_k \phi_k \Delta L = 1.$$

Equation (2.12) then gives

$$\phi_k \Delta L = \begin{cases} n_k/N_T, & L_k > L_{\min}(z_s), \\ 0, & L_k < L_{\min}(z_s). \end{cases}$$

where $n_k$ is the number of galaxies in the $k$th luminosity bin and $N_T$ is the total number of galaxies. The information matrix is

$$\mathbf{I}(\phi_k \Delta L) = \begin{bmatrix} -\delta_{ij} N_T/n_i + N_T + 1 & 1 \\ 1 & 0 \end{bmatrix},$$

and hence the components of the covariance matrix are

$$\text{var}\,(\phi_i \Delta L) = \frac{n_i(N_T - n_i)}{N_T^3},$$

$$\text{cov}\,(\phi_i \phi_j) = \frac{-n_i n_j}{N_T^3}, \qquad i \neq j,$$

as expected in the limit of large $n_i$.

## 2.2 TESTS OF THE METHODS

In this section we test various aspects of some of the methods described in Section 2.1 against Monte Carlo simulations of clustered and unclustered distributions. It is particularly important to check the maximum likelihood estimators in detail since such methods are usually biased. The simulations also allow us to test whether the asymptotic error estimates based on equations (2.7) and (2.13) are applicable to samples and bin sizes as small as those used in the analysis of the real data sets described in Section 3.

The Monte Carlo models have been generated to roughly match the sample size of the AARS (see Paper III). Set (A) consists of 40 simulations with an average of 322 points distributed uniformly amongst five fields each of area 3.75°×3.75°. Three fields were assigned a limiting magnitude $m_{\rm lim}=17.0$ and the other two were assigned $m_{\rm lim}=16.65$ and $m_{\rm lim}=16.75$ respectively. The points were generated with luminosities drawn from a Schechter function with parameters

$$\left.\begin{matrix} M^*=-19.65 \\ \alpha=-1.0 \end{matrix}\right\} -16.5>M>-22.5. \tag{2.14}$$

A $k$-term of $3.0z$ was applied to each point. Set (B) consists of 40 simulations with identical parameters to those of set (A) except that the points were distributed in a hierarchical fashion following the simple Soneira–Peebles (1977) prescription. The resulting models have clustering properties similar to those of the AARS with autocorrelation function $\xi(r)=(r_0/r)^{1.8}$, $r_0=4.5\,h^{-1}$ Mpc, $r\leqslant 8\,h^{-1}$ Mpc (see also Paper I, where a similar set of simulations was used to test clustering statistics).

In the first test we have applied equation (2.1) and fitted the counts $dN(L)$ by least-squares, thereby determining the three parameters of the Schechter function $\phi^*$, $M^*$, and $\alpha$. We used bin widths of $\Delta M=0.25$ mag or larger if the number of galaxies per 0.25 mag bin dropped below 5. The finite bin widths were taken into account in fitting equation (2.1). Results from this traditional least-squares method for the two sets of Monte Carlo simulations are listed in Table 1 (labelled TLS). In the second test we have applied the STY maximum likelihood method (equation 2.5). Corresponding results for this technique are also listed in Table 1. The points to notice are as follows:

(i) The TLS method is unbiased;

(ii) the TLS variances of the Schechter function parameters are substantially larger (by a factor of ~2) for hierarchically clustered distributions than for random points;

(iii) the STY method is slightly biased, tending to underestimate $M^*$, but the bias is substantially less than $1\sigma$;

**Table 1.** Tests of methods against Monte Carlo simulations.

**Set A (Uniform distribution)**

| | $\langle M^*\rangle$ | $\sigma(M^*)$ | $\langle\alpha\rangle$ | $\sigma(\alpha)$ | Corr($M^*$, $\alpha$) | $\times10^{-3}$ $\langle\phi^*\rangle$ | $\times10^{-3}$ $\sigma(\phi^*)$ | Corr($\phi^*$, $M^*$) | Corr($\phi^*$, $\alpha$) |
|---|---|---|---|---|---|---|---|---|---|
| TLS | -19.65 | 0.10 | -1.00 | 0.12 | 0.82 | 7.76 | 1.14 | 0.82 | 0.73 |
| STY | -19.63 | 0.16 | -0.99 | 0.16 | 0.78 | | | | |

**Set B (Hierarchical distribution)**

| | $\langle M^*\rangle$ | $\sigma(M^*)$ | $\langle\alpha\rangle$ | $\sigma(\alpha)$ | Corr($M^*$, $\alpha$) | $\times10^{-3}$ $\langle\phi^*\rangle$ | $\times10^{-3}$ $\sigma(\phi^*)$ | | |
|---|---|---|---|---|---|---|---|---|---|
| TLS | -19.65 | 0.18 | -0.97 | 0.27 | 0.84 | 8.21 | 2.24 | 0.81 | 0.55 |
| STY | -19.60 | 0.14 | -0.95 | 0.17 | 0.74 | | | | |

(iv) the variances of $M^*$ and $\alpha$ for the STY method are insensitive to the level of clustering but are larger than those for the least-squares method applied to an unclustered distribution. [The distribution of results in the $M^*-\alpha$ plane from the STY method is in excellent agreement with that inferred from equation (2.7)];

(v) in both methods $M^*$ and $\alpha$ are highly correlated; for the TLS method $\phi^*$ is also highly correlated with the other two parameters.

In Appendix A we derive expressions for the covariance matrix of $M^*$ and $\alpha$ which are in excellent agreement with the results listed in Table 1. We therefore conclude that for real data, such as the AARS and KOSS surveys which are obviously clustered, the STY method will give more reliable results than a 'traditional' method based on equation (2.1) which implicitly assumes a uniform distribution. For shallow catalogues, such as the CfA survey where the Local Supercluster presents a significant local overdensity, the use of a technique like the STY method is essential for sensible results.

We have also tested the stepwise maximum-likelihood method (hereafter SWML) described in Section 2.1.3 against the Monte Carlo simulations. One can see from equation (2.12), by taking the limit $\Delta L \rightarrow 0$, that each of the estimates $\phi_k$ is related to the true luminosity function $\phi(L)$ by

$$\phi_k \approx \frac{\int_{L_k-\Delta L/2}^{L_k+\Delta L/2} \phi \, dN(L)}{\int_{L_k-\Delta L/2}^{L_k+\Delta L/2} dN(L)} \approx \frac{\int \phi^2 L^{3/2} \, dL}{\int \phi L^{3/2} \, dL}. \tag{2.15}$$

Both sets of simulations give mean estimates of $\phi_k$ in good agreement with equation (2.15), with no evidence for significant bias. In addition, the standard deviations of the $\phi_k$ computed from equation (2.13) are in excellent agreement with the empirically determined standard deviations. This applies even when the mean number of galaxies per magnitude bin is as low as 3. For unclustered data it has larger variances than the TLS method, but as with the STY method, it is insensitive to the presence of clustering and is therefore substantially more reliable than the TLS method when applied to clustered data. The variances of the $\phi_k$ are weakly dependent on the value of the constant $\beta$ appearing in the constraint (equation 2.11). The quantity $\Sigma_k[\sigma(\phi_k)/\phi_k]^2$ is minimized for values of $\beta$ that typically lie within the range $1<\beta<3/2$, thus we adopt $\beta=3/2$ in the analysis of Section 3.

One of the main uses of this method is to provide a quantitative assessment of whether the Schechter function provides an acceptable fit to the luminosity function. A standard technique (e.g. Eadie *et al.* 1971) is to compute a likelihood ratio $\ln(\mathfrak{L}_1/\mathfrak{L}_2)$. In our case $\ln \mathfrak{L}_1$ is computed using the specified function and $\ln \mathfrak{L}_2$ is computed from equation (2.9) and the corresponding maximum likelihood solution for $\phi_k$. One should not, however, set $\mathfrak{L}_1$ equal to the exact likelihood used in the STY method, since this can lead to likelihood ratios which are large and negative. This is because the integral appearing in equation (2.5) is replaced by a summation over a (relatively small) number of discrete steps in equation (2.9). Since the accuracy with which the integrals are evaluated depends on the size of the luminosity interval $\Delta L$ (or the corresponding absolute magnitude interval $\Delta M$), the likelihood $\mathfrak{L}_2$ is sensitive to the size of the bin widths and thus also on the number of parameters $\phi_k$. A meaningful likelihood ratio test, which is insensitive to bin widths, can be devised provided that $\ln \mathfrak{L}_1$ is computed using equation (2.9) with the $\phi_k$ set equal to the values expected for a Schechter function as in equation (2.15). With $\mathfrak{L}_1$ computed in this way, $2\ln(\mathfrak{L}_1/\mathfrak{L}_2)$, is distributed asymptotically as $\chi^2$ with $N_p-1$ degrees of freedom, where $N_p$ is the total number of discrete $\phi_k$ values. [It is $\chi^2(N_p-1)$ rather than $\chi^2(N_p)$ because the arbitrary normalization of the $\phi_k$ effectively eliminates one free parameter via the linear constraint (2.11).] The accuracy of this asymptotic result, and the extent to which this test is independent of the size

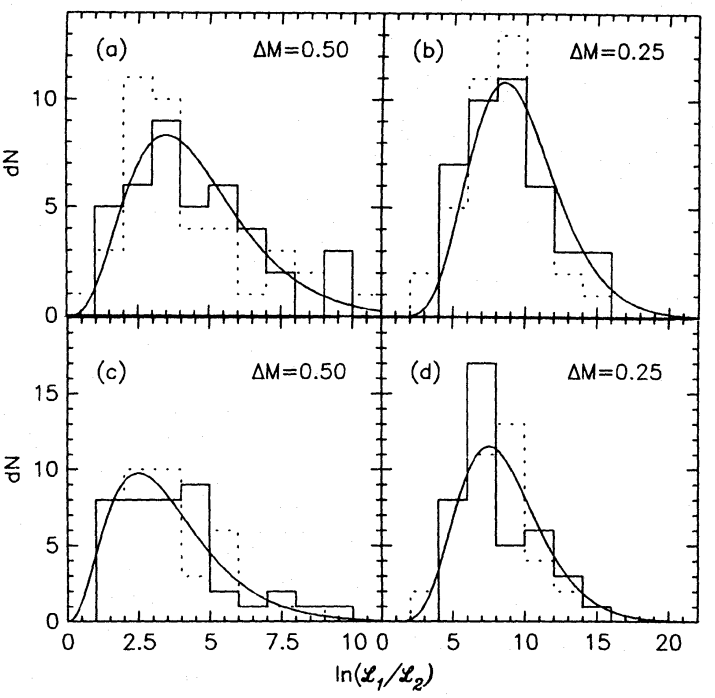


**Figure 2.** Frequency distribution of likelihood ratios for two sets of Monte Carlo simulations. Solid histograms show results for simulations in which galaxies where uniformly distributed and dotted histograms show results for hierarchically clustered galaxies. In (a) and (b) the likelihood $\mathfrak{L}_1$ is computed using the Schechter function parameters adopted in the simulations as described in Section 2.2 and the likelihood $\mathfrak{L}_2$ is computed from equation (2.9). The smooth curves show the expected distributions, i.e. that $2\ln(\mathfrak{L}_1/\mathfrak{L}_2)$ should be asymptotically distributed as $\chi^2$ with $N_p-1$ degrees of freedom, where $N_p$ is the total number of steps of $\phi_k$ (equation 2.8). Notice that the curves agree with the histograms for both choice of absolute magnitude interval $\Delta M=0.5$ and $\Delta M=0.25$. In (c) and (d) the likelihood $\mathfrak{L}_1$ is computed using the Schechter function parameters determined for each simulation using the STY method. The solid curves shown $\chi^2$ distributions with $N_p-3$ degrees of freedom.

of the bin widths is shown in Fig. 2(a) and (b), where we have computed the likelihood ratios for the two sets of Monte Carlo simulations. In practice, however, the Schechter function parameters will be determined from the same set of data (using, say, the STY method) as the $\phi_k$ and hence we expect that in this case the distribution of $2\ln(\mathfrak{L}_1/\mathfrak{L}_2)$ will be narrower than $\chi^2(N_p-1)$. The analysis of this problem is complicated, since the Schechter parameters are not simply related to the $\phi_k$. From the asymptotic properties of the likelihood function, we expect that the statistic $2\ln(\mathfrak{L}_1/\mathfrak{L}_2)$ should approach a distribution which lies between $\chi^2(N_p-3)$ and the distribution expected of

$$z=\sum_{i=1}^{N_p} x_i^2-\sum_{j=1}^{2} x_j^2,$$

where the $x_i$ are independent normal variates with unit variance. In practical applications where $N_p$ is large ($N_p\approx 10$–$24$), these distributions are similar, hence with little loss of accuracy we may adopt the $\chi^2(N_p-3)$ distribution to set confidence intervals on the acceptability of a Schechter function. This conclusion is confirmed from the Monte Carlo results shown in Fig. 2(c) and (d).

## 3 Luminosity functions

In this section we present estimates of the luminosity functions and Schechter function parameters for five redshift surveys. In each case we adopt the magnitude systems used to construct

the survey. A discussion of the transforms between these magnitude systems and an intercomparison of the luminosity functions is postponed until Section 4, where we also address the question of the normalization of the luminosity function. With the exception of the AARS analysed in Section 3.1, luminosity functions for these surveys have also been published by other authors. We therefore compare our results with previous analyses and discuss any discrepancies in detail. As mentioned in Section 2.1, the assumption that luminosity is uncorrelated with position or type is unlikely to be strictly correct. This assumption may be partly checked by analysing subsets of the galaxies which are known (or expected) to have different clustering properties. Thus, where possible, we present separate results for galaxies of different morphological type.

### 3.1 THE AARS

The AARs is fully described in Paper III. Here we summarize a few of the relevant details. The survey consists of about 340 galaxies in five fields each of area 3.75°×3.75°. The photographic photometry was done on short exposure UK Schmidt plates in the $B_J$ pass-band using Kodak IIIa-J photographic plates and a Schott GG395 glass filter. Zero-points were established using photoelectric measurements made in special filter bands (Couch & Newell 1980) that closely match the photographic combination. Following Shanks *et al.* (1984b), the zero-pointed isophotal magnitudes are denoted $B_J$. The isophotal limit corresponds approximately to 23.6 $B_J$ mag arcsec$^{-2}$.

Absolute magnitudes are computed assuming a uniform Hubble flow and the luminosity distance for a Friedmann model with $q_0=0.5$. The adopted $k$-corrections are listed in Table 2. Galactic absorption and internal reddening are ignored. The limiting magnitude for the AAT redshift sample varies slightly from field to field. To avoid bias in the luminosity function analysis it is important that each field should be complete to a chosen magnitude limit. As a consistency check we have applied the $V/V_{max}$ test (Schmidt 1968) to each of the fields with the results shown in Table 3. For a uniform distribution of galaxies $\langle V/V_{max}\rangle=0.5$ and the expected rms dispersion is $\sigma(V/V_{max})=1/\sqrt{12N}$ where $N$ is the number of objects in the field. For hierarchically clustered distributions, our Monte Carlo simulations suggest dispersions larger by a factor ~1.5 at $B_J\approx17$. Our adopted magnitude limits are indicated by the asterisks in Table 3. The $V/V_{max}$ tests are compatible with completeness within each field. Schechter function parameters have been determined with the STY method using galaxies with absolute magnitudes within the range $-22\leqslant M_{B_J}\leqslant-17$. The limit at faint absolute magnitudes is of no importance as only a few objects are excluded and they carry little weight in the solutions. The faint limit is included to facilitate comparison between the STY solutions and the SWML estimates. The limit at bright magnitudes should be viewed with some caution since it is clear from equation (2.5) that the weight assigned

**Table 2.** $k$-corrections.

| Galaxy type | $k$ $B_J$ | $k$ $J_{KOS}$ |
|---|---|---|
| E-S0 | 4.14 | 3.3 |
| Sa-Sb | 2.90 | 2.2 |
| Sc | 2.25 | 1.7 |
| Sd-Sm | 1.59 | 1.1 |

Note: $\Delta m=kz$.

**Table 3.** $V/V_{max}$ test.

(a) AARS $B_J$

| | Field | | | | |
|---|---|---|---|---|---|
| $m_{lim}$ | S1 | S2 | S3 | N1 | N2 |
| 17.0 | 0.57* | 0.52* | 0.41* | 0.59 | 0.62 |
| | (62) | (56) | (50) | (43) | (60) |
| 17.1 | 0.55 | 0.49 | 0.39 | 0.62 | 0.43* |
| | (68) | (60) | (52) | (55) | (65) |
| 17.2 | 0.49 | 0.46 | 0.38 | 0.57 | 0.40 |
| | (68) | (62) | (55) | (58) | (67) |
| 17.3 | 0.43 | 0.42 | 0.34 | 0.56* | 0.36 |
| | (68) | (63) | (55) | (65) | (67) |
| 17.4 | 0.39 | 0.37 | 0.30 | 0.52 | 0.31 |
| | (68) | (63) | (55) | (69) | (67) |

(b) KOS survey $J_{KOS}$

| | Field | | | | | | | |
|---|---|---|---|---|---|---|---|---|
| $m_{lim}$ | NP4 | NP5 | NP6 | NP7 | SP3 | SP4 | SP5 | SP6 |
| 15.0 | 0.47 | 0.69 | 0.53 | 0.60 | 0.52 | 0.56 | 0.46 | 0.45 |
| | (36) | (17) | (24) | (20) | (14) | (14) | (12) | (25) |

(c) KOSS survey $F_{KOS}$

| | Field | | | | | |
|---|---|---|---|---|---|---|
| $m_{lim}$ | NP5 | NP7 | NP8 | SP4 | SP5 | SP6 |
| 16.0 | 0.49 | 0.36 | 0.48 | 0.57 | 0.61* | 0.53* |
| | (53) | (24) | (31) | (28) | (30) | (27) |
| 16.1 | 0.49* | 0.34 | 0.47* | 0.54 | 0.60 | 0.48 |
| | (60) | (25) | (34) | (31) | (34) | (28) |
| 16.2 | 0.46 | 0.36 | 0.42 | 0.54 | 0.54 | 0.49 |
| | (63) | (27) | (34) | (35) | (35) | (32) |
| 16.3 | 0.41 | 0.41 | 0.39 | 0.49 | 0.55 | 0.51 |
| | (63) | (31) | (35) | (36) | (40) | (37) |
| 16.4 | 0.36 | 0.40 | 0.36 | 0.50* | 0.50 | 0.48 |
| | (63) | (33) | (36) | (41) | (41) | (39) |
| 16.5 | 0.32 | 0.42* | 0.32 | 0.45 | 0.45 | 0.46 |
| | (63) | (37) | (36) | (42) | (41) | (41) |

Notes: The numbers in brackets below each $V/V_{max}$ estimate give the total number of galaxies with measured redshifts brighter than the limiting magnitude $m_{lim}$. The asterisks mark the magnitude limits adopted for the AAT and KOSS fields.

to intrinsically bright galaxies is sensitive to whether the Schechter function provides an accurate description of the data. The bright end of the luminosity function is also extremely sensitive to magnitude errors. The effects of magnitude errors are discussed in further detail in Section 3.5 where we analyse the CfA survey. The deep redshift surveys are too small to give statistically significant results concerning the shape of the extreme bright end of the luminosity function, hence rather than risk biasing the results by including all bright galaxies our approach is to limit the range of absolute magnitudes to about 2 mag on either side of $M^*$. We then test whether the Schechter function provides an acceptable fit to the data by using the SWML method and the likelihood ratio test described in Section 2.2.

The Schechter function parameters for the AARS are given in Table 4. Corresponding error ellipses are shown in Fig. 3. The Schechter function fits are compared with the SWML estimates in Fig. 4. The results of the likelihood ratio tests (Table 4) show that the Schechter function

**Table 4.** Luminosity function parameters for deep field surveys.

(a) AARS

| Type | N | range | | $B_J^*$ | $\alpha$ | $\ln(\mathcal{L}_1/\mathcal{L}_2)$ | | $N_p$ |
|---|---|---|---|---|---|---|---|---|
| ALL | 291 | −22.0 | −17.0 | −19.56 | −1.04 | 8.0 | | 15 |
| E-S0 | 97 | −22.0 | −17.0 | −19.37 | −0.48 | 6.4 | (7.3) | 10 |
| S | 194 | −22.0 | −17.0 | −19.64 | −1.24 | 4.2 | (4.6) | 15 |

(b) KOS

| Type | N | range | | $J_{KOS}^*$ | $\alpha$ | $\ln(\mathcal{L}_1/\mathcal{L}_2)$ | | $N_p$ |
|---|---|---|---|---|---|---|---|---|
| ALL | 159 | −22.0 | −17.0 | −20.23 | −1.64 | 2.4 | | 10 |
| E-S0 | 77 | −22.0 | −17.0 | −20.01 | −1.04 | 2.3 | (3.5) | 10 |
| S | 82 | −22.0 | −17.0 | −19.87 | −1.72 | 1.2 | (0.7) | 10 |

| Type | N | range | | $F_{KOS}^*$ | $\alpha$ | $\ln(\mathcal{L}_1/\mathcal{L}_2)$ | | $N_p$ |
|---|---|---|---|---|---|---|---|---|
| ALL | 136 | −23.0 | −18.0 | −21.48 | −2.08 | 2.0 | | 10 |

(c) KOSS

| Type | N | range | | $F_{KOS}^*$ | $\alpha$ | $\ln(\mathcal{L}_1/\mathcal{L}_2)$ | | $N_p$ |
|---|---|---|---|---|---|---|---|---|
| ALL | 229 | −23.0 | −18.0 | −21.07 | −1.04 | 6.4 | | 15 |

| Type | N | range | | $J_{KOS}^*$ | $\alpha$ | $\ln(\mathcal{L}_1/\mathcal{L}_2)$ | | $N_p$ |
|---|---|---|---|---|---|---|---|---|
| ALL | 181 | −22.0 | −17.0 | −19.88 | −0.92 | 8.2 | | 15 |

Notes: $N$ lists the total number of galaxies used in the luminosity function estimates. The columns labelled range give the range of absolute magnitudes used. $M^*$ is given in the magnitude system of the original survey. $M^*$ and $\alpha$ are Schechter function parameters which maximize the likelihood in the STY method. $\mathrm{Ln}(\mathfrak{L}_1/\mathfrak{L}_2)$ lists the ratio of the likelihood $\mathfrak{L}_1$ (see Section 2.2) determined from the best-fitting Schechter function to the likelihood $\mathfrak{L}_2$ of the stepwise method with $N_p$ parameters described in Section 2.1.3. For the cases where we have analysed different morphological types we list in brackets the likelihood ratio using the Schechter function parameters determined from the whole survey.

provides an acceptable description of the luminosity within the range $-22 \leqslant M_B \leqslant -17$. In addition, the likelihood ratio tests confirm the results of Fig. 3 that the differences between the luminosity functions of early-type and late-type galaxies are not significant. The 'flat' faint-end slope for the AARS sample is supported by a recent (and quite different) analysis by Phillipps & Shanks (1987).

### 3.2 THE KOS SURVEY

The KOS sample contains approximately 160 galaxies in eight fields and is almost complete to a magnitude limit of $J_{KOS}=15$. The $J_{KOS}$ photometric system (Kodak IIIa-J photographic plate plus Wratten 4 gelatin film filter) differs considerably from that used in the AAT survey (see Paper III, section 4). In addition, KOS claim their magnitudes are close to total magnitudes. KOS also list $F_{KOS}$ magnitudes (Kodak 098 plate plus Schott RG610 filter) for most of the galaxies in the

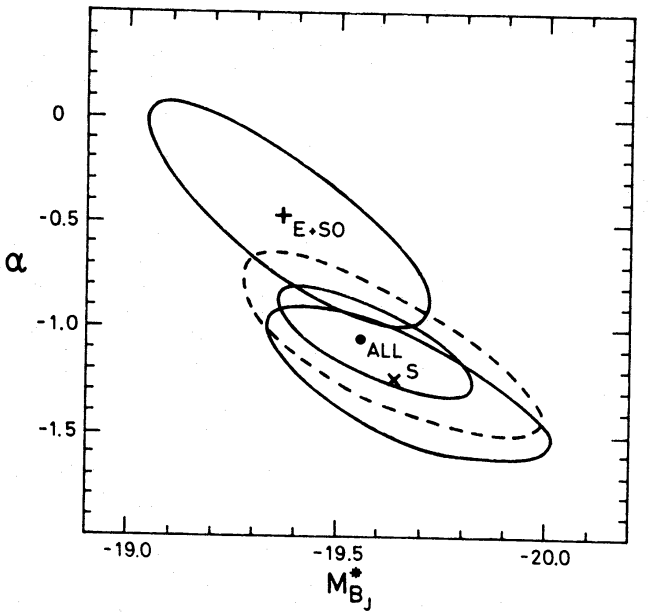


**Figure 3.** Error ellipses for the AARS luminosity function. Solid lines show 1$\sigma$ error contours. Dotted line shows a 2$\sigma$ error contour for all galaxy types.

sample. As a function of morphological type, $k$-corrections have been estimated for the $J_{KOS}$ system by one of us (RSE) and are listed in Table 2. KOSS pointed out that the $J$ magnitudes and $J-F$ colours listed in KOS for field NP5 are in error. We have corrected these using equations (5) and (6) in KOSS. In Table 3 we list $V/V_{max}$ for each field at the magnitude limit $J=15$. (We ignore the slight incompleteness at this limit.)

The best fitting Schechter function parameters are given in Table 4. Fig. 5 shows the error ellipses for the $J$ sample. We also list Schechter function parameters for the $F$-band luminosity

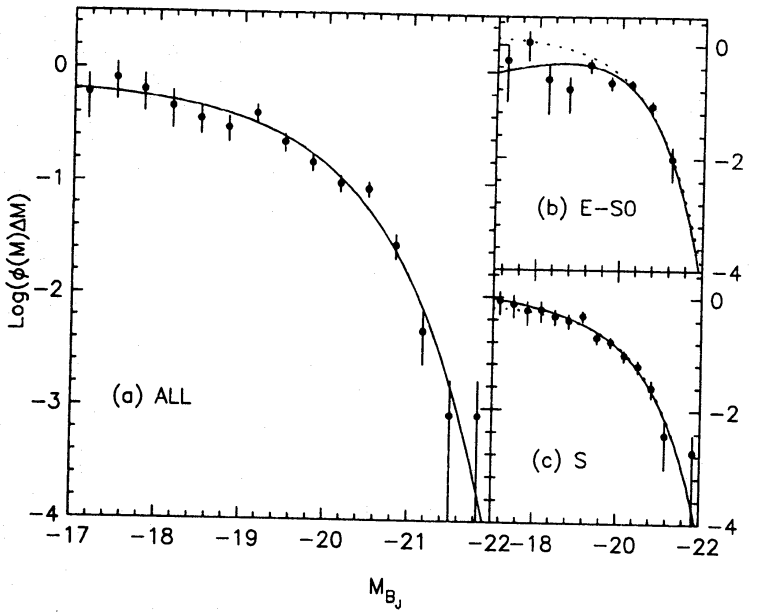


**Figure 4.** Luminosity functions for the AARS determined with the SWML method. The solid lines show the best-fitting Schechter function determined with the STY method. Dotted curves in (b) and (c) show the best fit for the whole sample [solid line in (a)].

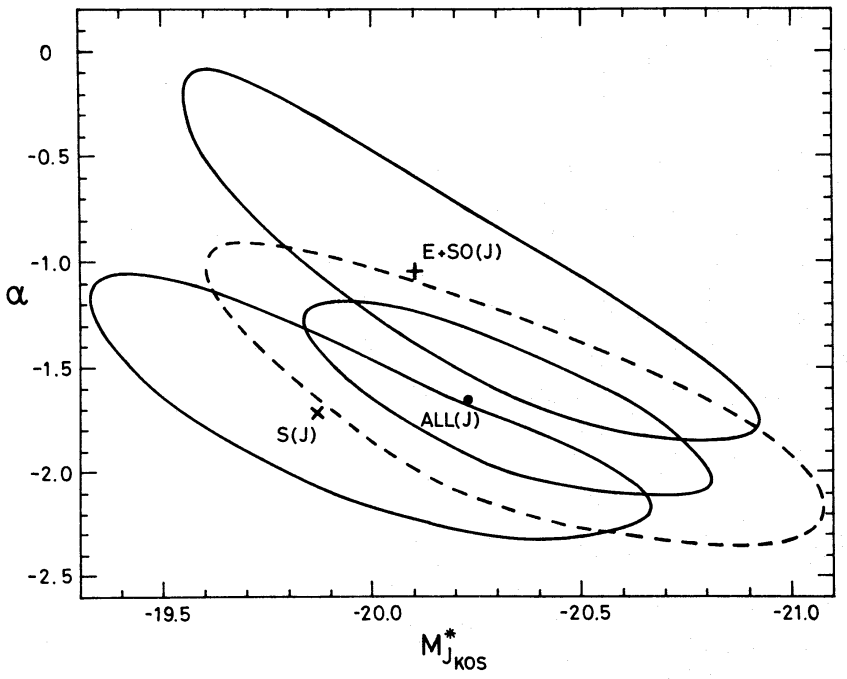


**Figure 5.** Error ellipses for the KOS survey luminosity function. Solid lines show $1\sigma$ error contours. Dotted line shows a $2\sigma$ error contour for all galaxy types.

function determined from a subsample of the KOS survey with the following limits in $F$: NP4, 13.83; NP5, 14.14; NP6, 14.14; NP7, 13.87; SP4, 13.92; SP5, 13.87; SP6, 13.70. For the $F$ magnitudes we used the $k$-corrections described by KOSS. The SWML method is compared with the Schechter function fits in Fig. 6 where open circles represent the $F$ magnitudes, closed circles the $J$ magnitudes. The Schechter function provides a good description of the data and this is confirmed by the likelihood ratios listed in Table 4.

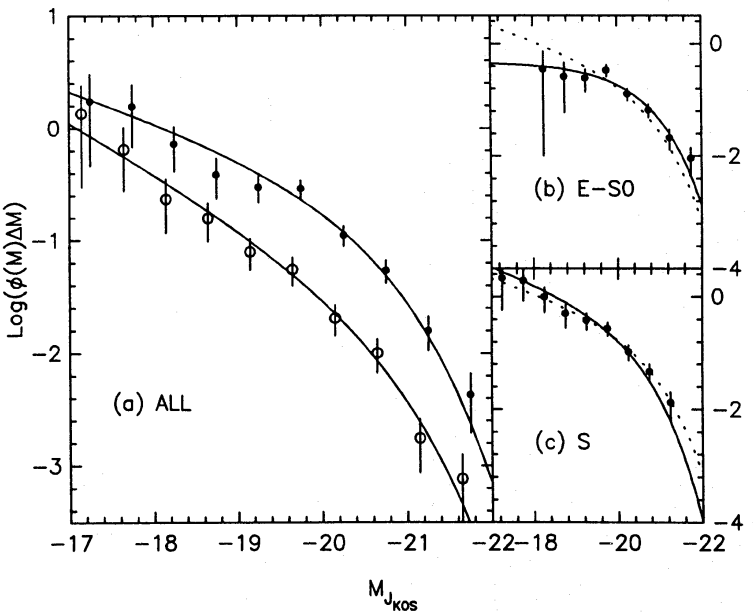


**Figure 6.** Luminosity functions for the KOS survey determined with the SWML method. Filled circles show results for the $J_{KOS}$-band, open circles show results for the $F_{KOS}$-band displaced towards faint magnitudes by 1.1 mag for clarity. The solid lines show the best-fitting Schechter function determined with the STY method. Dotted curves in (b) and (c) show the best fit for the whole $J_{KOS}$ sample [solid line in (a)].

The parameters given here differ considerably from those listed in KOS ($M^*_{J_{KOS}}=-19.68\pm0.20$, $\alpha=-1.36\pm0.29$, after correction for differences in Hubble constant and our neglect of galactic absorption). The main cause of the discrepancy arises partly from differences in estimation technique but mostly from the revisions in the magnitudes for field NP5. The inclusion of $k$-corrections causes little difference. The solutions determined by KOSS for this sample ($M^*_{J_{KOS}}=-19.94$, $\alpha=-1.54$; $M^*_{F_{KOS}}=-21.40$, $\alpha=-1.70$; computed from solutions 1 and 7 in table III of KOSS) are much closer to ours and lie within our $1\sigma$ error ellipses. The key discrepancy between our analysis and the revised analysis of KOSS concerns the sizes of the error ellipses. Our analysis suggests that KOSS have underestimated their errors. As we will show below, the steep faint end slope of the KOS luminosity function $\alpha\approx-1.6$ is not characteristic of the luminosity function determined from the deeper KOSS survey, or with the other luminosity functions described in this paper. As Fig. 6 shows, the galaxies contributing to this steep slope in the solutions lie within the range $-18<M_J<-17$. There are only eight galaxies in the $J$ sample with absolute magnitudes within this range so it does not seem unreasonable that the $2\sigma$ error ellipse shown in Fig. 5 permits values of $\alpha$ as large as $\alpha\approx-0.8$. As with the AARS, the differences between the luminosity functions of early- and late-type galaxies in this survey are not significant.

### 3.3 THE KOSS SURVEY

KOSS extended the original KOS survey to about a limit of $F_{KOS}\approx16$ in six small fields containing ~280 galaxies. The degree of overlap with the KOS sample is small, so it is a good approximation to treat the KOSS sample as an independent survey. $V/V_{max}$ for each field is listed in Table 3 as a function of limiting magnitude in the $F$-band. Our adopted magnitude limits are indicated by the asterisks. We have also analysed a $J$-limited subsample with the following magnitude limits: NP5, 16.80; NP7, 17.23; NP8, 16.81; SP4, 16.88; SP5, 16.99; SP6, 16.96. As morphological types are not listed for the KOSS galaxies, we have used the colour-dependent $k$-corrections given by KOSS.

The luminosity function results are given in Table 4 and in Figs 7 and 8. KOSS list four Schechter function solutions. With the exception of their solution 2 (KOSS, table III) their

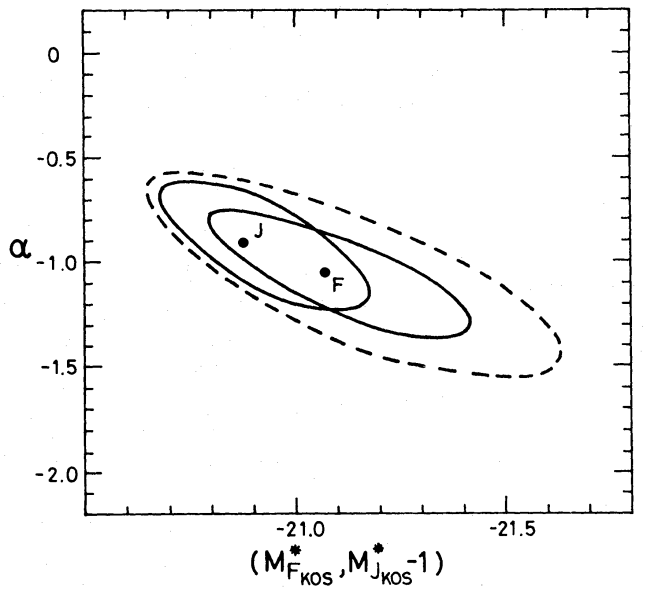


**Figure 7.** Error ellipses for the KOSS survey luminosity function. Solid lines show $1\sigma$ error contours. Dotted line shows a $2\sigma$ error contour for the $F_{KOS}$ sample.

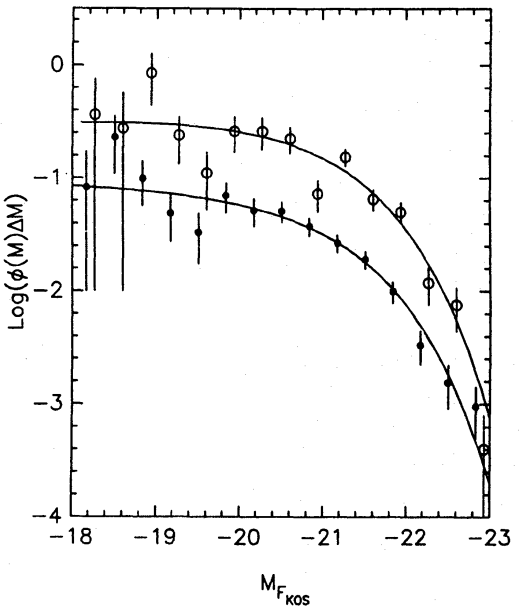


**Figure 8.** Luminosity functions for the KOSS survey determined with the SWML method. Filled circles show results for the $F_{KOS}$-band, open circles show results for the $J_{KOS}$-band displaced towards bright magnitudes by 1.1 mag for clarity. The solid lines show the best-fitting Schechter function determined with the STY method.

parameters lie within our $1\sigma$ error ellipses. KOSS noted that their solutions were sensitive to the inclusion or exclusion of two luminous galaxies in A1775. In our solutions, one of these is brighter than our cut-off at $M_{F_{KOS}}=-23$. There are two additional galaxies brighter than this limit, both of which have higher redshifts than the limit of 35 000 km s$^{-1}$ imposed by KOSS. If we include these three bright galaxies in our analysis, the best-fitting Schechter function parameters become $M^*_{F_{KOS}}=-21.31$, $\alpha=-1.20$. This solution still lies well within our $1\sigma$ error ellipse.

### 3.4 THE RSA CATALOGUE

In this section we describe an analysis of the RSA sample (Sandage & Tammann 1981). This sample was supplemented by a redshift catalogue compiled by Dr J. Huchra (private communication) which is similar to the RSA except that it is limited to $B(0)=13.2$. We cross-correlated all galaxies in these two catalogues which satisfied the criteria $B_T\leqslant 12.5$, $|b|\geqslant 30°$. The mean magnitude difference is

$$B_T=B(0)-0.29, \qquad \sigma=0.20 \tag{3.1}$$

with a weak dependence on morphological type [$B_T-B(0)=0.51$ for E-S0, $B_T-B(0)=0.22$ for Sc-I]. This relation is useful in comparing earlier results based mostly on the $B(0)$ system of the *Reference Catalogue of Bright Galaxies* (de Vaucouleurs & de Vaucouleurs 1964) with the present analysis (*cf.* Felten 1977, 1985). Thirty galaxies in Huchra's catalogue were not listed in the RSA but satisfied the condition $B_T\leqslant 12.5$ according to equation (3.1). They were included in the final sample. The RSA is known to become progressively incomplete at $B_T>12.5$. According to the analysis of Tammann *et al.* (1979) the incompleteness of the catalogue as a whole may be approximated by the function $f(m)=\{\exp[(m-m_L)/\Delta m_L]+1\}^{-1}$ with $m_L=12.83$, $\Delta m_L=0.16$. This suggests that the incompleteness at $B_T<12.5$ is small and we neglect it in the analysis below. It seems preferable to limit the catalogue at a well-defined magnitude limit rather than to include a parametric incompleteness function in the fit which would introduce correlations with the luminosity function parameters. As we show below, the errors introduced into the analysis by a

small degree of incompleteness are likely to be smaller than systematic errors associated with estimating distances to these nearby galaxies. Since we include galaxies at relatively low galactic latitudes we correct for galactic absorption using the model

$$\Delta m_B = A\,(\mathrm{cosec}\, b - 1), \qquad A = 0.13. \tag{3.2}$$

We adopt a linear Virgo-infall model based on equation (2) of Schechter (1980) with $\gamma = 2$. The mean recession velocity of the Virgo cluster is taken to be 1019 km s$^{-1}$ and the distance modulus of Virgo is fixed by the assumed infall velocity together with the requirement that the far-field Hubble constant be equal to 100 km s$^{-1}$ Mpc$^{-1}$. Galaxies with radial velocities less than 2500 km s$^{-1}$ and angles less than 6° from the centre of Virgo were assigned the distance of Virgo. All galaxies with recession velocities <500 km s$^{-1}$ are excluded from the analysis to minimize distance errors arising from peculiar velocities. The solution of the equation describing Virgo infall leads to triple-valued distances for a small number of galaxies. We have arbitrarily chosen the middle solution, though nearly identical results are obtained if these galaxies are excluded. It is certainly not worthwhile constructing a more refined infall model since the true flow pattern is likely to be complex within the triple valued region, with substantial departures from spherical symmetry. As a check on the influence of the central Virgo region, we also present results for samples in which all galaxies within 20° of the centre of Virgo are excluded.

The results for Schechter function fits over the range $-22 \leqslant M_B \leqslant -17$ are presented in Table 5. (Note that there are no galaxies brighter than the cut-off at $M_{B_T} = -22$.) The main difference between our analysis and previous work is that we find brighter values for $M^*_{B_T}$. For example, Schechter's (1976) analysis of a sample limited at $B(0) = 11.75$ gives $M^*_{B_T} = -19.26$, $\alpha = -1.24$, after corrections for differences in absorption and photometric systems. The analysis of galaxies with $B_T \leqslant 12.05$, $|b| > 40°$ from the *Second Reference Catalogue of Bright Galaxies* (de Vaucouleurs *et al.* 1976, hereafter RC2) described by KOS gives $M^*_{B_T} = -19.28$, $\alpha = -1.02$. Tammann *et al.* (1979) find $M^*_{B_T} = -19.19$, $\alpha = -1.03$. All of these determinations ignore Virgo infall.

Measurements of Virgo infall have been reviewed by Davis & Peebles (1983b), Dressler (1984) and Yahil (1985). Most determinations lie within the range $100 < v_I < 450$ km s$^{-1}$ with a probable 'best estimate' of $v_I \approx 300$ km s$^{-1}$. We therefore adopt our results for $v_I = 300$ km s$^{-1}$ in the comparison with the deep surveys described in Section 4.

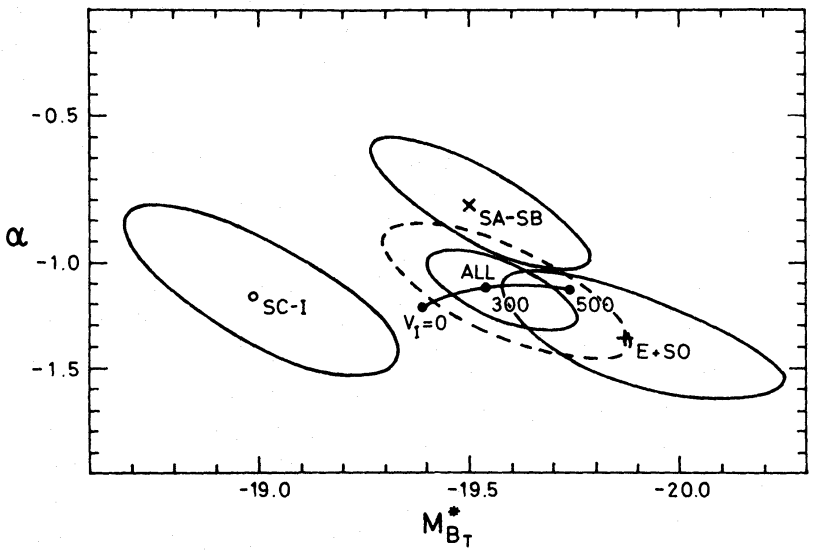


**Figure 9.** Error ellipses for the RSA sample limited at $B_T = 12.5$ and $|b| \geqslant 30°$. These results include a correction for galactic absorption ($A = 0.13$) and 'Virgo infall' ($v_I = 300$ km s$^{-1}$). The effect of changing 'Virgo-infall' on the luminosity function for all RSA galaxies is shown by the line joining the points labelled $v_I = 0$ and 500 km s$^{-1}$.

**Table 5.** Luminosity function parameters for the RSA survey.

| Sample | $m_{lim}$ | $v_I$ | $\|b\|$ | $A$ | N | $B_T^*$ | $\alpha$ | $\ln(\mathcal{L}_1/\mathcal{L}_2)$ | | $N_p$ |
|---|---|---|---|---|---|---|---|---|---|---|
| All | 12.0 | 0 | 30 | 0.13 | 346 | −19.54 | −1.44 | 2.3 | (6.6) | 15 |
| −Virgo | 12.0 | 0 | 30 | 0.13 | 263 | −19.51 | −1.44 | 4.3 | (6.9) | 15 |
| All | 12.0 | 300 | 30 | 0.13 | 345 | −19.81 | −1.44 | 3.7 | (5.1) | 15 |
| −Virgo | 12.0 | 300 | 30 | 0.13 | 263 | −19.68 | −1.40 | 6.2 | (7.5) | 15 |
| All | 12.0 | 500 | 30 | 0.13 | 346 | −19.94 | −1.40 | 2.9 | (5.5) | 15 |
| All | 12.0 | 300 | 30 | 0.0 | 345 | −19.78 | −1.44 | 4.5 | (6.2) | 15 |
| All | 12.0 | 300 | 40 | 0.0 | 315 | −19.79 | −1.40 | 4.1 | (5.0) | 15 |
| All | 12.5 | 0 | 30 | 0.13 | 587 | −19.39 | −1.20 | 5.0 | (9.1) | 15 |
| −Virgo | 12.5 | 0 | 30 | 0.13 | 453 | −19.29 | −1.08 | 4.3 | (6.9) | 15 |
| *All | 12.5 | 300 | 30 | 0.13 | 588 | −19.56 | −1.12 | 4.7 | | 15 |
| −Virgo | 12.5 | 300 | 30 | 0.13 | 454 | −19.50 | −1.08 | 5.3 | (5.6) | 15 |
| All | 12.5 | 500 | 30 | 0.13 | 590 | −19.74 | −1.12 | 2.5 | (5.5) | 15 |
| All | 12.5 | 300 | 30 | 0.0 | 588 | −19.56 | −1.16 | 4.1 | (4.4) | 15 |
| All | 12.5 | 300 | 40 | 0.0 | 524 | −19.54 | −1.08 | 2.7 | (2.8) | 15 |
| E+S0 | 12.5 | 300 | 30 | 0.13 | 192 | −19.87 | −1.36 | 3.8 | (4.8) | 15 |
| SA-SB | 12.5 | 300 | 30 | 0.13 | 230 | −19.50 | −0.72 | 1.1 | (9.5) | 15 |
| SC-I | 12.5 | 300 | 30 | 0.13 | 166 | −18.98 | −1.16 | 4.6 | (13.1) | 15 |

Notes: Schechter function parameters for the RSA sample in the $B_T$ system. $m_{lim}$ is the limiting magnitude, $v_I$ denotes the adopted 'Virgo-infall' velocity, $|b|$ lists the absolute value of the galactic latitude limit, $A$ is the absorption coefficient in equation (3.2). The remaining columns are as for Table 4. In the samples labelled (−Virgo) all galaxies within 20° of the centre of Virgo have been excluded from the analysis. The likelihood ratios listed in brackets have been computed using the Schechter function parameters of the asterisked solution.

Luminosity functions for galaxies grouped according to morphological type are shown in Fig. 10(b)–(d). The likelihood-ratio tests for the E-S0 and Sa-Sb luminosity functions show that they are compatible with the overall luminosity function for the sample. The luminosity function for late-type spirals (Sc-I) does have a significantly fainter value of $M^*_{B_T}$. The likelihood-ratio tests, and the plots shown in Fig. 10, demonstrate that the Schechter function provides an excellent description of the RSA luminosity functions.

### 3.5 THE CfA SURVEY

Our analysis of the CfA survey is similar to that of the RSA catalogue. However, the sample size is so large (~2000 galaxies) that systematic uncertainties in the Zwicky magnitude system and in the Virgo-infall model are much larger than the random errors. We therefore do not display error ellipses for this sample. The luminosity functions are shown in Fig. 11 and the Schechter function parameters are listed in Table 6. The results for no Virgo infall are in good agreement with those of Davis & Huchra (1982, $M^*_Z=-19.2$, $\alpha=-0.9$) and Choloniewski (1986, $M^*_Z=-19.20$, $\alpha=-1.09$). The likelihood ratio tests show that the CfA luminosity function differs significantly from a Schechter form. From Fig. 11(a) one can see that the CfA luminosity function changes slope more abruptly at $M_Z\approx-19$ than the best-fitting Schechter function and that there is an excess of bright galaxies at $M_Z<-21$. The discrepancy with a Schechter function at the bright end has been noted by Davis *et al.* (1983). Schechter function parameters for different morphological types are listed in Table 6. These show no major differences from the luminosity function for the whole sample. The most surprising result is that the luminosity function for late-type spirals (Sd-I) is so similar to the overall luminosity function.

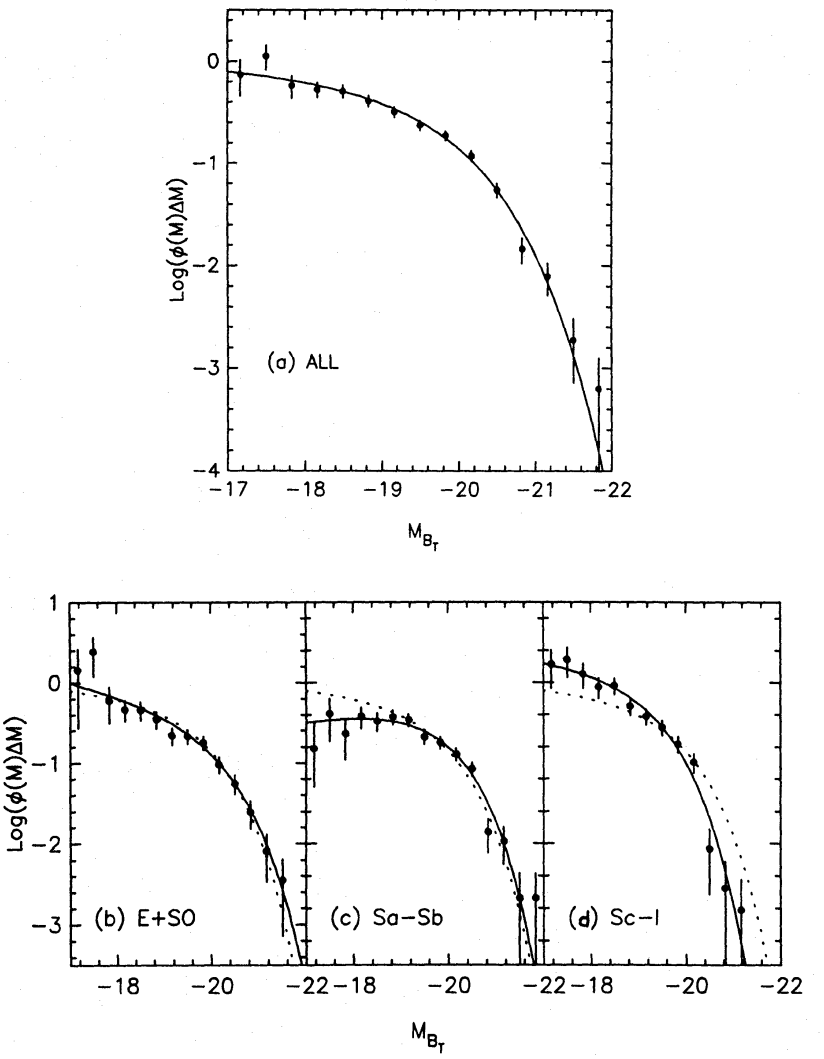


**Figure 10.** Luminosity functions for the RSA catalogue corresponding to the error ellipses shown in Fig. 9. Solid lines show the best-fitting Schechter functions. Dotted curves in (b)–(d) show the best fit for the whole sample [solid line in (a)].

The apparent discrepancies with the results from the RSA and deep surveys might be explained by errors in the Zwicky magnitudes. In Table 7 we give results of a comparison between $B_T$ magnitudes for galaxies listed in both the RC2 and the Zwicky catalogue. We have limited the comparison to galaxies with apparent magnitudes $13.5<B_T<14.5$ in order to coincide approximately with the magnitude range of galaxies in the CfA survey. These results indicate a dispersion of $\sigma(m)\approx 0.4$ mag, nearly all of which is likely to be attributable to errors in the Zwicky magnitudes. [Auman, Hickson & Fahlman (1982) have shown that some of this scatter is correlated with surface brightness.] The large errors in the Zwicky magnitudes will introduce a significant systematic bias in the luminosity function, especially at the bright end where it falls steeply. If we describe the magnitude errors by a Gaussian distribution, then the luminosity function appearing in equation (2.5) is related to the true luminosity function $\phi_T$ by the convolution

$$\phi(M)=\frac{1}{\sqrt{2\pi}\sigma(M)}\int_{-\infty}^{\infty}\phi_T(M')\exp\left[-\frac{(M'-M)^2}{2\sigma^2(M)}\right]dM'. \tag{3.3}$$

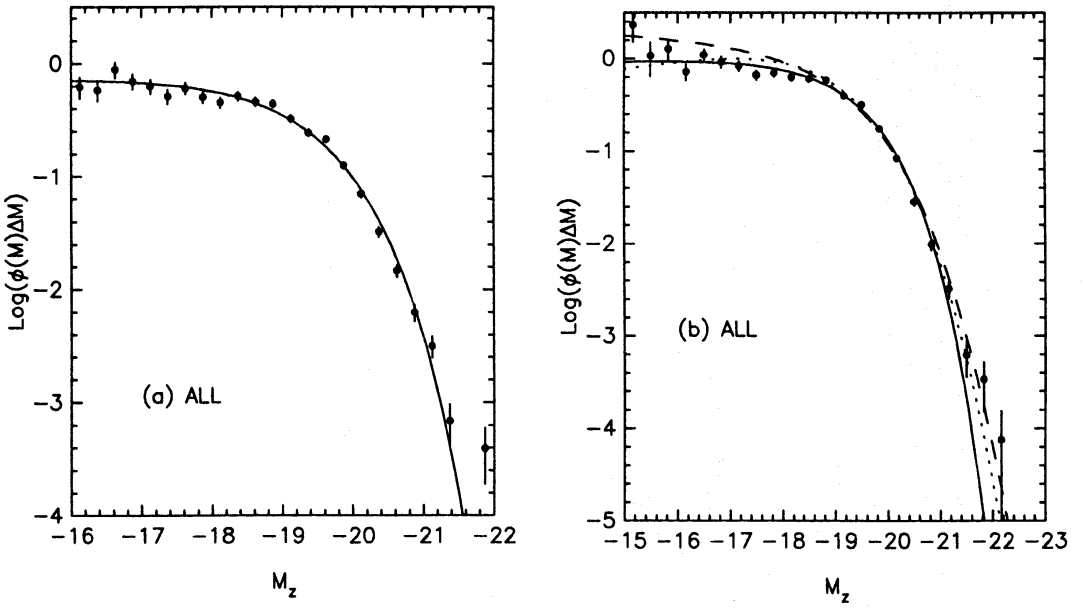


**Figure 11.** Luminosity functions for the CfA survey. (a) The SWML estimate for the asterisked sample in Table 6 and the line show the best-fitting Schechter function. The SWML estimate for a wider range of magnitudes. The solid line is as in (a). The dotted line shows the best-fitting Schechter function assuming that the magnitude errors are Gaussian distributed with a dispersion of $\sigma(m)=0.4$ mag. The dashed line shows the best-fitting Schechter function with $\sigma(m)=0.4$ mag and $\alpha$ constrained at $-1.1$.

In Fig. 12 we show examples of how such convolutions alter the shape of the luminosity function. This diagram clearly illustrates how magnitude errors affect the bright end and provides a justification of our procedure of limiting the range of absolute magnitudes over which we fit Schechter functions. While it is quite likely that there are some very luminous galaxies which cannot be described by the Schechter function, these are extremely rare in field surveys and are difficult to distinguish from galaxies with large magnitude errors (unless there is some clear morphological characteristic which is expected to correlate with total luminosity). This problem is

**Table 6.** Luminosity function parameters for the CfA sample.

| Sample | $m_{lim}$ | $v_I$ | N | $M_Z^*$ | $\alpha$ | $\ln(\mathcal{L}_1/\mathcal{L}_2)$ | $N_p$ |
|---|---|---|---|---|---|---|---|
| All | 14.0 | 0 | 1291 | -19.09 | -1.12 | 23.8 | 18 |
| All | 14.0 | 300 | 1272 | -19.15 | -0.92 | 18.8 | 18 |
| - Virgo | 14.0 | 300 | 933 | -19.06 | -0.80 | 22.7 | 18 |
| All | 14.0 | 500 | 1278 | -19.29 | -0.92 | 21.9 | 18 |
| All | 14.5 | 0 | 2201 | -19.10 | -1.08 | 21.9 | 24 |
| *All | 14.5 | 300 | 2259 | -19.16 | -0.96 | 28.7 | 24 |
| - Virgo | 14.5 | 300 | 1740 | -19.08 | -0.88 | 35.5 | 24 |
| All | 14.5 | 500 | 2276 | -19.23 | -0.92 | 28.0 | 24 |
| E+S0 | 14.5 | 300 | 635 | -19.23 | -0.88 | 10.3 | 18 |
| S | 14.5 | 300 | 1624 | -19.09 | -0.96 | 18.5 | 18 |
| E | 14.5 | 300 | 225 | -19.55 | -0.92 | 9.4 | 18 |
| S0 | 14.5 | 300 | 321 | -19.00 | -0.84 | 13.9 | 18 |
| S0/a-Sab | 14.5 | 300 | 475 | -18.99 | -1.00 | 10.5 | 18 |
| Sb-Sbc | 14.5 | 300 | 463 | -19.06 | -0.44 | 1.1 | 18 |
| Sc | 14.5 | 300 | 282 | -19.34 | -1.00 | 9.4 | 18 |
| Sd-I | 14.5 | 300 | 160 | -19.29 | -1.20 | 6.5 | 12 |

**Table 7.** Comparison of $B_T$ and $m_Z$ Zwicky magnitudes.

| Sample | $N$ | $\langle m_Z - B_T \rangle$ | $\sigma(m)$ |
|---|---|---|---|
| Vol I | 26 | 0.42 | 0.49 |
| Vol II | 30 | 0.39 | 0.39 |
| Vol III | 21 | 0.19 | 0.37 |
| Vol IV | 15 | 0.01 | 0.37 |
| Vol V | 22 | 0.28 | 0.37 |
| Vol VI | 25 | 0.28 | 0.39 |
| All | 139 | 0.29 | 0.41 |

Notes: Results are presented by Zwicky volume number (see Zwicky *et al.* 1961–68) for all RC2 galaxies with $13.5<B_T<14.5$. $N$ lists the number of galaxies in each sample. The columns labelled $\langle m_Z - B_T \rangle$ and $\sigma(m)$ list the mean magnitude difference and dispersion respectively.

even more severe if the magnitude errors follow a distribution which has a longer tail than a Gaussian. To test the effects of magnitude errors on the CfA results, we have fitted the model (3.3) with $\sigma(m)=0.4$. The results for the 14.5 mag limited sample with $v_l=300\,\mathrm{km\,s^{-1}}$ are $M_Z^*=-18.72$, $\alpha=-0.76$. This fit is shown as the dotted line in Fig. 11(b). The fit is reasonable in the region $M_Z\approx-19$, corresponding to the points with the smallest errors but it fails to match the points at fainter magnitudes. As expected, the likelihood ratio test shows that this fit can be rejected at a very high level of significance (<0.1 per cent). The dashed line in Fig. 11(b) shows the best fit with $\alpha$ constrained at $\alpha=-1.1$ (Section 4.1). This gives $M_Z^*=-19.01$, but overestimates the luminosity function in the range $-17>M_Z>-19$. In either case, these models are consistent with the CfA luminosity function at $M_Z<-19$, indicating that the excess bright galaxies may be understood in terms of magnitude errors with $\sigma(m)=0.4$. In detail, these models fail to

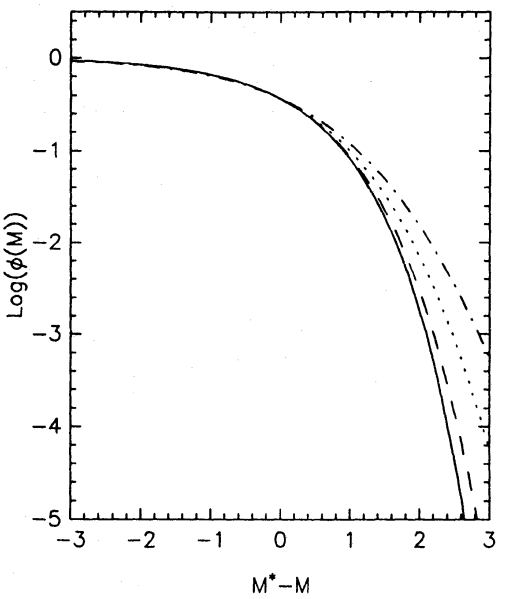


**Figure 12.** Effect of magnitude errors on the shape of the luminosity function in a volume-limited survey. The solid line shows a Schechter function with $\alpha=-1$. The other lines show this function convolved with a Gaussian of dispersion $\sigma(m)=0.2$ mag (dashed line), 0.4 mag (dotted line), 0.6 mag (dot-dashed line).

match the faint end of the luminosity function. This could indicate significant departures from a Schechter function, or from our simplified Gaussian model for the magnitude errors. Clearly more accurate magnitudes for the CfA galaxies are required to solve this problem.

## 4 Comparison of the luminosity functions and the mean luminosity density of the Universe

### 4.1 COMPARISON OF THE LUMINOSITY FUNCTIONS

In this section we present an intercomparison of the luminosity functions determined in Section 3. Any such comparison must be viewed as approximate since it is difficult to precisely correct for the different photometric systems. In detail, the transforms between these systems will contain colour (or morphological type) terms, complex isophotal corrections, etc. We realize that the procedure of transforming $M^*$ from one system into another by adding a constant offset is a gross oversimplification. However, since the sizes of the error ellipses determined in Section 3 are so large, and the differences between the luminosity functions of different morphological type are small, we do no great injustice to the data by adopting this simple approach. We transform the various photometric systems into the $B_T$ system according to the following relations,

$$B_T = m_Z - 0.29, \quad \text{(Table 7)} \tag{4.1a}$$

$$B_T = J_{KOS} + 0.35, \quad \text{(KOS)} \tag{4.1b}$$

$$B_T = F_{KOS} + 1.35, \tag{4.1c}$$

$$B_T = B_J - 0.29, \quad \text{(Paper III)}. \tag{4.1d}$$

The transform (4.1b) was deduced by KOS using the Zwicky catalogue as an intermediary between the $B_T$ system and their photometry. Equation (4.1c) is based on equation (4.1b) and the mean value $\langle J-F\rangle_{KOS}=1.0$ from the KOSS survey. Equation (4.1d) is probably the most poorly determined transform, relying on an empirical comparison between the AARS and KOS photometry together with equation (4.1b). In Appendix B we show that the empirical transform is in reasonable agreement with that expected for a typical spiral disc with corrections for different isophotes and pass-bands. Fig. 13 shows error ellipses from Figs 3, 5, 7 and 9 superimposed according the equations (4.1). We have not plotted results for the CfA catalogue because of the large systematic uncertainties in the luminosity function described in Section 3.5. Fig. 13 shows that the luminosity functions from all the surveys are broadly consistent with each other. It is

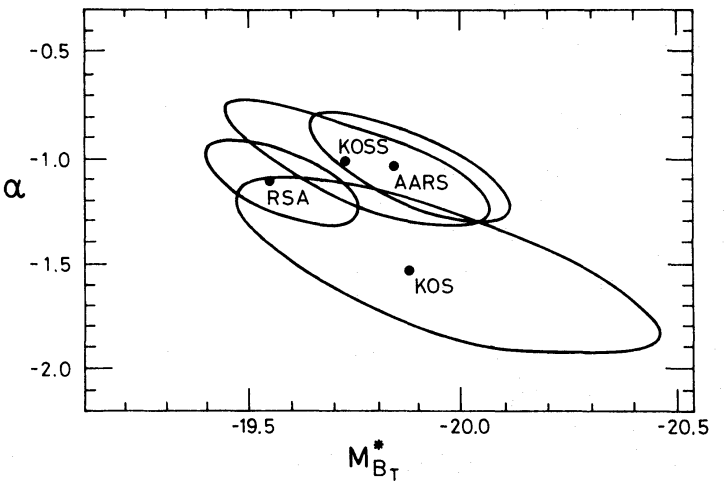


**Figure 13.** Error ellipse from Figs (3), (5), (7) and (9) transformed to the $B_T$ system according to equations (4.1).

difficult to assign a significance level to this result because the uncertainties in equations (4.1) are poorly known.

The mean of the faint-end slopes for the AAT, KOSS($F$) and RSA samples (asterisked solution in Table 5) is $\alpha=-1.07$. A reasonable estimate of the faint-end slope is thus

$$\alpha=-1.07\pm0.05, \tag{4.2}$$

where the error represents a rough estimate of the standard deviation. The steep faint-end slope of the KOS luminosity function is ignored in this estimate, but this is justified because faint galaxies carry little weight in the maximum-likelihood solution. Combining the likelihoods for the KOS($J$) and KOSS($J$) samples we find a maximum at $M^*_{J_{\rm KOS}}=-19.98$, $\alpha=-1.17$, consistent with equation (4.2). In Table 8 we list the maximum likelihood solutions for $M^*$ for each survey (together with $2\sigma$ errors) with $\alpha$ constrained at $\alpha=-1.1$. Ignoring the CfA survey, the mean value of the estimates for $M^*_{B_{\rm T}}$ is

$$M^*_{B_{\rm T}}=-19.68\pm0.10, \tag{4.3}$$

where the error is the standard deviation of the mean. This procedure seems appropriate because the errors in the transforms are likely to be at least as large as the random errors on each individual determination of $M^*$. In the case of the RSA catalogue, the systematic uncertainties associated with the Virgo-infall model are of about the same size as the random errors.

### 4.2 NORMALIZATION AND THE MEAN LUMINOSITY DENSITY OF THE UNIVERSE

Since the luminosity functions from each of the surveys have very similar functional forms, the values of $\phi^*$ determined from each survey should be directly comparable and independent of uncertainties in the transforms between photometric systems (*cf.* Loh & Spillar 1986). We use two methods to estimate the normalization $\phi^*$. The first is based on an unbiased, minimum variance estimator of the mean space density of galaxies (Davis & Huchra 1982). Consider galaxies with luminosities in the range $L_1<L<L_2$. The probability that a galaxy at distance $x$ is included in the catalogue is

$$S(x)=\frac{\displaystyle\int_{\min[L_{\min}(x),\,L_1]}^{L_2}\phi(L)\,dL}{\displaystyle\int_{L_1}^{L_2}\phi(L)\,dL}.$$

**Table 8.** Comparison of surveys.

| Survey | $M^*$ | $B^*_{\rm T}$ |
|---|---|---|
| AARS $B_J$ | −19.61±0.18 | −19.90 |
| KOS $J_{\rm KOS}$ | −19.84±0.24 | −19.49 |
| KOSS $F_{\rm KOS}$ | −21.12±0.20 | −19.77 |
| RSA $B_{\rm T}$ | −19.55±0.14 | −19.55 |
| CfA(1) $M_Z$ | −19.26±0.08 | −19.55 |
| CfA(2) $M_Z$ | −19.01±0.08 | −19.30 |

Notes: RSA results for asterisked sample in Table 5. CfA(1) as for asterisked sample in Table 6 with no correction for magnitude errors. CfA(2) as for CfA(1) except magnitude errors were included in the likelihood solutions as described in Section 3.5. The estimates of $M^*$ have been converted into the $B_{\rm T}$ system according to equations (4.1).

For a Schechter function, an estimate of $\phi^*$ is

$$\phi^* = \frac{\frac{1}{V}\sum_i \frac{1}{S(x_i)}}{\Gamma(\alpha+1, L_1/L^*) - \Gamma(\alpha+1, L_2/L^*)}, \tag{4.4}$$

where the sum extends over all galaxies within volume $V$.

A second estimate is based on fits to the number counts in each survey. Let $dN(m)$ be the number of galaxies per unit solid angle counted in the magnitude interval $(m, m+dm)$. The integral counts are given by

$$N(m) = \int_0^\infty \frac{y^2\, dy}{\sqrt{1-(H_0 y)^2(2q_0-1)}} \int_{L_{\min}(y)}^\infty \phi(L)\, dL = \phi^* I(m),$$

where

$$H_0 y = \frac{1-q_0+q_0 z+(q_0-1)\sqrt{1+2q_0 z}}{q_0^2(1+z)}$$

(Peebles 1980). If we minimize

$$\sum_n \frac{[dN(m_n)-\phi^*\, dI(m_n)]^2}{\phi^*\, dI(m_n)}$$

**Table 9.** Normalization.

| Survey | $\times 10^4 h^{-3}$Mpc$^3$ $V$ | Equation 4.4 $\times 10^{-2} h^3$ Mpc$^{-3}$ $\phi^*$ | $\sigma$ | Equation 4.5 $\times 10^{-2} h^3$ Mpc$^{-3}$ $\phi^*$ | $\sigma$ |
|---|---|---|---|---|---|
| AARS $B_J$ | 7.7 | $0.74^{+0.24}_{-0.15}$ | 0.20 | $0.83^{+0.17}_{-0.16}$ | 0.17 |
| KOS $J_{KOS}$ | 2.2 | $2.73^{+1.65}_{-0.87}$ | 1.70 | $2.39^{+0.52}_{-0.16}$ | 0.72 |
| KOSS $F_{KOS}$ | 2.1 | $1.45^{+0.41}_{-0.25}$ | 0.82 | $1.54^{+0.50}_{-0.23}$ | 0.49 |
| RSA(North) $B_T$ | 4.8 | $1.97^{+0.56}_{-0.40}$ | | | |
| RSA(South) $B_T$ | 4.8 | $0.76^{+0.21}_{-0.15}$ | | | |
| CfA(North) $M_Z$ | 31.4 | $1.86^{+0.33}_{-0.27}$ | | $2.60^{+0.30}_{-0.26}$ | |
| | | 2.07* | | 2.99* | |
| CfA(South) $M_Z$ | 14.4 | $1.32^{+0.21}_{-0.17}$ | | $1.73^{+0.19}_{-0.28}$ | |
| | | 1.46* | | 1.98* | |

Notes: AARS, $v_{max}=22\,000\,km\,s^{-1}$, $-22<B_J<-17$. KOS, $v_{max}=12\,000\,km\,s^{-1}$, $-22<J_{KOS}<-17$. KOSS, $v_{max}=26\,000\,km\,s^{-1}$, $-23<F_{KOS}<-17$. RSA, $v_l=300\,km\,s^{-1}$, $|b|<40°$. $v_{max}=4000\,km\,s^{-1}$, $-22<B_T<-18.5$. CfA, $v_l=300\,km\,s^{-1}$, $v_{max}=8000\,km\,s^{-1}$, $-22<M_Z<-18.5$. $V$ denotes the effective volume of each survey, $V=\frac{1}{3}\omega(V_{max}/H_0)^3$, where $\omega$ is the solid angle of the survey. The $\pm$ errors on $\phi^*$ indicate the changes caused by varying $M^*$ over the ranges listed in Table 8 with $\alpha=-1.1$. The numbers in the columns headed $\sigma$ list the standard deviation in $\phi^*$ for each individual field in the deep surveys determined from the field-to-field fluctuations. The Zwicky number counts were fitted over the range $12.0<m_Z<15.5$. For the CfA sample, the estimates of $\phi^*$ marked with * were determined with $\alpha=-0.96$, $M_Z^*=-19.16$.

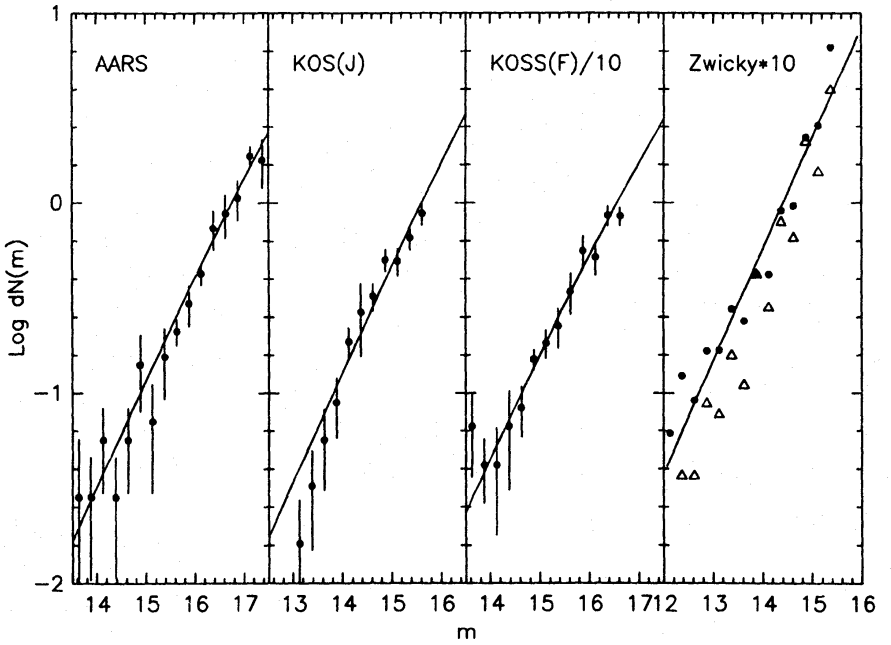


**Figure 14.** $dN(m)$ is the number of galaxies deg$^{-2}$ (0.25 mag)$^{-1}$. The lines are the predicted number counts normalized by the least-squares fit (equation 4.5) for each survey. These were computed assuming a mean $k$-term for the deep surveys [$kz$, where $k$=3.0 for AARS, $k$=2.5 for KOS($J_{KOS}$) and $k$=1.5 for KOSS($F_{KOS}$)]. The error bars are computed from the field-to-field fluctuations. For the Zwicky catalogue filled circles show counts in the north and open triangles show counts in the south. The KOSS counts have been divided by 10 and the Zwicky counts have been multiplied by 10.

with respect to $\phi^*$, where the sum extends over the total number of apparent magnitude bins, we find

$$\phi^{*2}=\frac{\sum_n [dN(m_n)]^2/dI(m_n)}{\sum_n dI(m_n)}. \tag{4.5}$$

Table 9 lists results for $\phi^*$ based on equations (4.4) and (4.5) using the values of $M^*$ listed in Table 8 together with $\alpha=-1.1$. To reduce any bias caused by the large number of intrinsically faint nearby galaxies in the RSA and CfA surveys, we have integrated equation (4.4) only over those galaxies with $-22<M<-18.5$. In fact, the results are quite stable and do not change significantly if the faint limit is reduced to $M=-17.0$. Fig. 14 shows the number counts for the AARS, KOS, KOSS and Zwicky catalogues together with the predicted counts (see the figure caption for further details). The results from equation (4.5) are slightly higher than those from equation (4.4) as expected from the bias caused by the Local Supercluster. However the dispersion amongst the estimates is extraordinarily large. In particular, the best estimate of $\phi^*$ for the AARS is a factor of 2 lower than the mean, while $\phi^*$ for the KOS sample is nearly a factor of 2 higher than the mean. The expected variance in the number density (and therefore $\phi^*$ for a luminosity function of a standard form) is given approximately by

$$\frac{\delta n}{n}\sim\left(4\pi\int_0^\infty \xi(x)x^2\,dx/V\right)^{1/2}, \tag{4.6}$$

(Davis & Huchra 1982) where $V$ is the 'effective' volume of each survey (see Table 9). The variance is therefore sensitive to the shape of the two-point galaxy correlation function $\xi(x)$ at

large scales. The integral $4\pi J_3=\int \xi(x)d^3x$ is thought to lie in the range 3000–10 000 $h^{-3}$ Mpc$^3$ (Davis & Peebles 1983a). The large fluctuations in Table 9 may therefore reflect a value of $4\pi J_3$ at the upper end of this range. The AARS is marginally consistent with this hypothesis if uncertainties in the selection function are also taken into account. An alternative possibility is that the large fluctuations in $\phi^*$ are caused by systematic errors in the magnitudes or completeness of the surveys, but neither the shapes of the luminosity functions nor the $V/V_{max}$ tests provide any evidence in favour of this.

To obtain a final value of $\phi^*$ we have averaged the results from equation (4.4) weighting by $1/\sqrt{V}$. We have ignored the RSA sample as it is not independent of the CfA survey. The result is

$$\phi^*=(1.56\pm0.34)\times10^{-2}h^3\,\mathrm{Mpc}^{-3}. \tag{4.7}$$

This estimate is close to the mean for the north and south subsets of the CfA survey. The mean luminosity density implied by equations (4.2), (4.6) and (4.7) is

$$\langle L_B\rangle=\phi^*\Gamma(\alpha+2)L^*\approx(1.93^{+0.8}_{-0.6})\times10^8\,h\,L_\odot.$$

(assuming $M_{B_\odot}=5.48$) and therefore the mass-to-light ratio required to close the Universe is

$$(M/L)_{crit}=(1500^{+700}_{-400})\,h(M/L)_\odot$$

well in excess of the typical mass-to-light ratios of groups and rich clusters [$\approx$100–400 $h(M/L)$, see e.g. Dressler 1978; Faber & Gallagher 1979; Huchra & Geller 1982; Colless 1987].

## 5 Conclusions

Our main conclusions are as follows:

(i) We have described and tested maximum-likelihood methods for estimating the luminosity function in field surveys of clustered galaxies. The methods are nearly unbiased and have reliably determined errors. The stepwise maximum-likelihood allows an accurate goodness-of-fit test for simple parametric forms of the luminosity function.

(ii) These methods have been applied to five redshift surveys. Apart from the CfA survey, the luminosity functions are found to be well described by Schechter functions and are compatible with each other.

(iii) There is no evidence for differences in the luminosity functions for morphological types earlier than Sc in the bandpasses considered here. The luminosity function for types Sc-I has a fainter $M^*$ than for earlier types. We find no strong evidence for a maximum in any of the luminosity functions at $M_{B_T}\leqslant-17.0$.

(iv) The luminosity function for the CfA sample does not fit a Schechter function. Part of the discrepancy is caused by an excess of bright galaxies. We have argued that this may be caused by random errors in the Zwicky magnitude system.

(v) We conclude that in the $B_T$ system, the field luminosity function may be described by a Schechter function with parameters $\alpha=-1.07\pm0.05$, $M^*_{B_T}=-19.68\pm0.10$, $\phi^*=(1.56\pm0.34)\times10^{-2}$ Mpc$^3$ (for $H_0=100$ km s$^{-1}$ Mpc$^{-1}$).

Our current state of knowledge of the luminosity function is unsatisfactory in several respects. The error ellipses shown in Fig. 13 are large. Furthermore, since we lack accurate transforms between the various magnitude systems, one cannot significantly improve the results by combining surveys. The situation could be improved by a systematic programme of photometry. It would be particularly useful to obtain accurate magnitudes and colours for the CfA galaxies. It would also be of great value to construct a new redshift survey containing about 500–1000 galaxies limited to $B_J\approx17$ following the random sampling strategy advocated by Kaiser (1986). This would

substantially reduce the errors in the luminosity function parameters (Table 1, Appendix A) and would provide an accurate measurement of the mean space density of galaxies ($\delta n/n \leqslant 5$ per cent) because of the large volume surveyed. The field surveys provide only limited results on the morphological-type dependence of the luminosity function and give essentially no useful constraints for magnitudes $M_{B_T} \geqslant -16$. This problem is of particular relevance for studies of deep number counts (Ellis 1987). One approach is to study the luminosity functions according to morphological type and colour in nearby rich clusters (Sandage *et al.* 1985). The problem here is that even if one is willing to assume that the shape of each separate luminosity function is independent of environment, one also requires the appropriate normalizations for a field sample. A large photometric survey to moderately deep limiting magnitudes ($B_J \approx 17$) in two or more colours together with a random sampled redshift survey would be one way of tackling this problem. Another approach, based on cross-correlating bright ($B_J \sim 17$) galaxies with measured redshifts with much fainter galaxies ($B_J \sim 20$) has been discussed by Phillipps & Shanks (1987).

## Acknowledgments

We thank J. Choloniewski, O. Lahav and P. J. E. Peebles for their comments on a draft of this paper. We also thank our colleagues who have worked on various aspects of the AARS, A. J. Bean, R. Fong, T. Shanks and Z. Zen-Long. This work was supported by the Nuffield Foundation.

## References

Abramowitz, M. & Stegun, I. A. (eds), 1970. *Handbook of Mathematical Functions,* p. 267, Dover Publishing Inc., New York.

Auman, J. R., Hickson, P. & Fahlman, G. G., 1982. *Publs astr. Soc. Pacif.*, **94,** 9.

Bean, A. J., Efstathiou, G., Ellis, R. S. & Shanks, T., 1983. *Mon. Not. R. astr. Soc.*, **205,** 605 (Paper I).

Blair, M. & Gilmore, G., 1982. *Publs astr. Soc. Pacif.*, **94,** 742.

Choloniewski, J., 1986. *Mon. Not. R. astr. Soc.*, **223,** 1.

Colless, M., 1987. *PhD thesis,* University of Cambridge.

Couch, W. J. & Newell, E. B., 1980. *Publs astr. Soc. Pacif.*, **92,** 746.

Davis, M. & Huchra, J., 1982. *Astrophys. J.*, **254,** 437.

Davis, M. & Peebles, P. J. E., 1983a. *Astrophys. J.*, **267,** 465.

Davis, M. & Peebles, P. J. E., 1983b. *Ann. Rev. Astr. Astrophys.*, **21,** 109.

Davis, M., Huchra, J. & Latham, D., 1983. In: *The Early Evolution of the Universe and its Present Structure, IAU Symp. No. 104,* eds Abell, G. O. & Chincarini, G., Reidel, Dordrecht, Holland.

de Vaucouleurs, G. & de Vaucouleurs, A., 1964. *Reference Catalogue of Bright Galaxies,* University of Texas Press, Austin, Texas.

de Vaucouleurs, G., de Vaucouleurs, A. & Corwin, H. G., 1976. *Second Reference Catalogue of Bright Galaxies,* University of Texas Press, Austin, Texas (RC2).

Dressler, A., 1978. *Astrophys. J.*, **226,** 55.

Dressler, A., 1980. *Astrophys. J.*, **236,** 351.

Dressler, A., 1984. *Astrophys. J.*, **281,** 512.

Eadie, W. T., Drijard, D., James, F. E., Roos, M. & Sandoulet, B., 1971. *Statistical Methods in Experimenting Physics,* North Holland, Amsterdam.

Ellis, R. S., 1983. In: *The Origin and Evolution of Galaxies,* eds Jones, B. J. T. & Jones, J. E., Reidel, Dordrecht, Holland.

Ellis, R. S., 1987. In: *Observational Cosmology, IAU Symp. No. 124,* ed. Burbidge, G., Reidel, Dordrecht, Holland.

Faber, S. M. & Gallagher, J. S., 1979. *Ann. Rev. Astr. Astrophys.*, **17,** 135.

Felten, J. E., 1977. *Astr. J.*, **82,** 861.

Felten, J. E., 1985. *Commts Astrophys.*, **11,** 53.

Frenk, C. S., White, S. D. M., Davis, M. & Efstathiou, G., 1988. *Astrophys. J.*, in press.

Groth, E. J. & Peebles, P. J. E., 1977. *Astrophys. J.*, **217,** 385.

Huchra, J. P. & Geller, M. J., 1982. *Astrophys. J.*, **257,** 423.
Huchra, J. P., Davis, M., Latham, D. & Tonry, J., 1983. *Astrophys. J. Suppl.*, **52,** 89.
Jackson, J. C., 1974. *Mon., Not. R. astr. Soc.*, **166,** 281.
Kaiser, N., 1986. *Mon. Not. R. astr. Soc.*, **219,** 785.
Kendall, M. G. & Stuart, A., 1961. *The Advanced Theory of Statistics,* Vol. 2, Griffin & Griffin, London.
Kirshner, R. P., Oemler, A. & Schechter, P. L., 1978. *Astr. J.*, **83,** 1549.
Kirshner, R. P., Oemler, A. & Schechter, P. L., 1979. *Astr. J.*, **84,** 951 (KOS).
Kirshner, R. P., Oemler, A., Schechter, P. L. & Schectman, S. A., 1983. *Astr. J.*, **88,** 1285 (KOSS).
Kraan-Korteweg, R. C., Sandage, A. & Tammann, G. A., 1984. *Astrophys. J.*, **283,** 24.
Lawrence, A., Walker, D., Rowan-Robinson, M., Leech, K. J. & Penston, M. V., 1986. *Mon. Not. R. astr. Soc.*, **219,** 687.
Loh, E. D. & Spillar, E. J., 1986. *Astrophys. J.*, **307,** L1.
Lynden-Bell, D., 1971. *Mon. Not. R. astr. Soc.*, **155,** 95.
Peebles, P. J. E., 1980. *The Large-Scale Structure of the Universe,* Princeton University Press, Princeton.
Peterson, B. A., Ellis, R. S., Efstathiou, G., Shanks, T., Bean, A. J., Fong, R. & Zen-Long, Z., 1986. *Mon. Not. R. astr. Soc.*, **221,** 233 (Paper III).
Peterson, B. A., Ellis, R. S., Kibblewhite, E. Hooley, A. & Horne, D., 1979. *Astrophys. J.*, **233,** L109.
Phillipps, S. & Shanks, T., 1987. *Mon. Not. R. astr. Soc.*, **227,** 115.
Sandage, A. & Tammann, G. A., 1981. *A Revised Shapley–Ames Catalog of Bright Galaxies,* Carnegie Institution of Washington.
Sandage, A., Binggeli, B. & Tammann, G. A., 1985. *Proc. ESO Workshop on the Virgo Cluster of Galaxies,* eds Richter, O.-G. & Binggeli, B., ESO.
Sandage, A., Tammann, G. A. & Yahil, A., 1979. *Astrophys. J.*, **232,** 352 (STY).
Schechter, P. L., 1976. *Astrophys. J.*, **203,** 297.
Schechter, P. L., 1980. *Astr. J.*, **85,** 801.
Schmidt, M., 1968. *Astrophys. J.*, **151,** 393.
Shanks, T., Bean, A. J., Efstathiou, G., Ellis, R. S., Fong, R. & Peterson, B. A., 1984a. *Astrophys. J.*, **274,** 529.
Shanks, T., Stevenson, P. R. F., Fong, R. & MacGillivray, H. T., 1984b. *Mon. Not. R. astr. Soc.*, **206,** 767.
Soneira, R. M. & Peebles, P. J. E., 1977. *Astrophys. J.*, **211,** 1.
Tammann, G. A., Yahil, A. & Sandage, A., 1979. *Astrophys. J.*, **234,** 775.
Turner, E. L., 1979. *Astrophys. J.*, **203,** 297.
van der Kruit, P. C., 1987. *Astr. Astrophys.*, **173,** 59.
White, S. D. M. & Rees, M. J., 1978. *Mon. Not. R. astr. Soc.*, **183,** 341.
Yahil, A., 1985. *Proc. ESO Workshop on the Virgo Cluster of Galaxies,* eds Richter, O.-G. & Binggeli, B., ESO.
Zwicky, F., Herzog, E., Wild, P., Karpowicz, M. & Kowal, C., 1961–1968. *Catalog of Galaxies and Clusters of Galaxies, Vols I–VI,* California Institute of Technology, Pasadena.

## Appendix A: Error analysis for maximum-likelihood estimators

In this appendix we briefly discuss error estimates for maximum likelihood methods. We assume a luminosity function of the Schechter form and derive asymptotic formulae for the covariance matrix of the parameters $M^*$ and $\alpha$. To simplify the analysis we ignore $k$-corrections and relativistic effects. We first consider the case when galaxies are uniformly distributed in space (Section A1). In this case, the analysis is straightforward and the final answers provide useful estimates of the variances expected in a redshift survey of sample size $N$ (particularly if a random sampling strategy is adopted so that the assumption of a uniform spatial distribution of galaxies is not too far from the truth). In Section A2 we summarize a similar analysis of the STY estimator which largely explains the error behaviour found from the Monte Carlo simulations in Section 2.2.

### A.1 MAXIMUM LIKELIHOOD ESTIMATOR FOR A UNIFORM DISTRIBUTION OF GALAXIES

In Section 2.2 we applied a 'traditional' (i.e. assuming that galaxies are uniformly distributed in space) method of estimating $\phi(L)$ using least-squares fits to the formula (2.1). A maximum likelihood method for tackling this problem may easily be formulated; the individual probabilities

appearing in the likelihood function may be written as

$$p_i \propto \phi(L_i)V(L_i, m_{\rm lim}) \Big/ \int_0^\infty \phi(L)V(L, m_{\rm lim})\, dL. \tag{A1}$$

The Schechter function parameters which maximize the likelihood function are the solutions of the equations

$$L^* = \frac{1}{(\alpha+5/2)N} \sum_i L_i, \tag{A2a}$$

$$\psi(\alpha+5/2) = \frac{1}{N} \sum_i \ln (L_i/L^*), \tag{A2b}$$

where $\psi$ is the digamma function and the summations extend over the $N$ galaxies in the sample. The information matrix $\mathbf{I} = -(\partial^2 \ln \mathfrak{L}/\partial\theta^2)$ may readily be written down and inverted to yield

$$\text{var}\,(L^*) = \frac{1}{N} \frac{\psi'(\alpha+5/2)L^{*2}}{(\alpha+5/2)\psi'(\alpha+5/2)-1}, \tag{A3a}$$

$$\text{var}\,(\alpha) = \frac{1}{N} \frac{\alpha+5/2}{(\alpha+5/2)\psi'(\alpha+5/2)-1}, \tag{A3b}$$

$$\text{cov}\,(\alpha, L^*) = -\frac{1}{N} \frac{L^*}{(\alpha+5/2)\psi'(\alpha+5/2)-1}, \tag{A3c}$$

where $\psi' = d\psi/d\alpha$. [Note that to convert to magnitude $M^*$ on the left-hand side of equations (A3a–c) replace $L^*$ on the right-hand side by $-(0.4 \ln 10)^{-1}$.] Tables of the digamma function and its derivative are conveniently listed in Abramowitz & Stegun (1970), thus equations (A3a–c) may be readily evaluated for values of $\alpha$ in the range of most interest. Table A1 lists answers for several values of $\alpha$. Notice the excellent agreement between the results for $\alpha = -1$ and those listed in Table 1 for the least-squares 'traditional' estimator (which is statistically similar to the above method) deduced from the Monte Carlo simulations in which galaxies were distributed uniformly at random.

**Table A1.** Evaluation of the components of the covariance matrices for the two maximum-likelihood methods described in Appendix A. The values listed are for $N=300$.

| | Equations (A3a–c) | | | Equations (A5a–c) | | |
|---|---|---|---|---|---|---|
| $\alpha$ | $\sigma(M^*)$ | $\sigma(\alpha)$ | Corr $(\alpha, M^*)$ | $\sigma(M^*)$ | $\sigma(\alpha)$ | Corr $(\alpha, M^*)$ |
| 0.0 | 0.092 | 0.19 | 0.90 | 0.12 | 0.24 | 0.86 |
| −0.5 | 0.094 | 0.15 | 0.88 | 0.13 | 0.20 | 0.82 |
| −1.0 | 0.096 | 0.11 | 0.84 | 0.14 | 0.17 | 0.77 |
| −1.5 | 0.100 | 0.072 | 0.78 | 0.16 | 0.13 | 0.68 |

## A.2 ANALYSIS FOR STY MAXIMUM-LIKELIHOOD ESTIMATOR

In this case the likelihood equation gives

$$\frac{\partial \ln \mathfrak{L}}{\partial L^*} = -\frac{(\alpha+1)N}{L^*} + \sum_i \frac{L_i}{L^{*2}} - \sum_i \frac{\partial \ln \Gamma[\alpha+1, L_{\rm min}(z_i)/L^*]}{\partial L^*} = 0, \tag{A4a}$$

$$\frac{\partial \ln \mathfrak{L}}{\partial \alpha} = \sum_i \ln L_i - N \ln L^* - \sum_i \frac{\partial \ln \Gamma[\alpha+1, L_{\rm min}(z_i)/L^*]}{\partial \alpha} = 0. \tag{A4b}$$

The expectation values of the terms containing the incomplete gamma functions can easily be evaluated and thus equations (A4a, b) can be shown to reduce to equations (A2a, b) in the limit of large $N$. The components of the information matrix are more complicated in this case. One obtains

$$E\left(\frac{\partial^2 \ln}{\partial L^{*2}}\right)=-\left[\alpha+\frac{19}{4}-\frac{3}{2}\frac{I_1(\alpha)}{\Gamma(\alpha+5/2)}\right]\frac{N}{L^{*2}}, \tag{A5a}$$

$$E\left(\frac{\partial^2 \ln \mathfrak{L}}{\partial \alpha^2}\right)=-\left[\psi'(\alpha+5/2)+\psi^2(\alpha+5/2)-\frac{3}{2}\frac{I_2(\alpha)}{\Gamma(\alpha+5/2)}\right]N, \tag{A5b}$$

$$E\left(\frac{\partial^2 \ln \mathfrak{L}}{\partial \alpha \partial L^*}\right)=-\left[1+\frac{3}{2}\psi(\alpha+5/2)-\frac{3}{2}\frac{I_3(\alpha)}{\Gamma(\alpha+5/2)}\right]\frac{N}{L^*}, \tag{A5c}$$

where the integrals $I_1$, $I_2$, and $I_3$ are

$$I_1=\int_0^\infty \frac{x^{2\alpha+5/2}\exp(-2x)}{\Gamma(\alpha+1, x)}\,dx,$$

$$I_2=\int_0^\infty \frac{x^{1/2}g^2(x)}{\Gamma(\alpha+1, x)}\,dx,$$

$$I_3=\int_0^\infty \frac{g(x)x^{\alpha+3/2}\exp(-x)}{\Gamma(\alpha+1, x)}\,dx,$$

and

$$g(x)=\int_0^\infty z^\alpha \ln z \exp(-z)\,dz.$$

We have evaluated equations (A5a–c) for several values of $\alpha$ and computed the components of the covariance matrix. The results are listed in Table A1. Notice that the asymptotic variances for the STY estimator are in excellent agreement with the Monte Carlo simulations described in Section 2.2 and that they are larger than those determined from equations (A3a–c). This behaviour is easy to understand for as noted above the solutions of the likelihood equations for the method described in Section A1 differ from equations (A4) in that the summations over the incomplete gamma functions are replaced by their expectation values for a uniform distribution of galaxies. We would therefore expect that the STY estimator will yield larger errors when applied to a uniform distribution of galaxies and this is confirmed by the analysis presented here.

## Appendix B: Isophotal correction for $B_J$ magnitudes

For an exponential disc the correction from an isophotal magnitude at isophote $\Sigma_J(x)$ to total magnitude is

$$B_J(T)-B_J(x)=2.5\log[1-(1+x)\exp(-x)] \tag{B1a}$$

$$x=\frac{\Sigma_J(x)-\Sigma_J(0)}{1.09} \tag{B1b}$$

where $\Sigma_J(0)$ is the central surface brightness of the disc. van der Kruit (1987) has recently determined the mean face-on central surface brightness for spiral discs in a $J$ system similar to ours (IIIa-J plate and Wratten 2 filter). Correcting his result to random inclinations and correct-

ing for the small difference in photometric system (Blair & Gilmore 1982; van der Kruit 1987), we find $\Sigma_J(0)\approx 21.05$ mag arcsec$^{-2}$. For the AARS photometry $\Sigma_J(x)=23.6$, thus

$$B_J(T)-B_J(23.6)=-0.4. \tag{B2}$$

The photographic $J$ system is related to the $J_{KOS}$ system by

$$J=J_{KOS}-0.11+0.41(J-F)_{KOS} \tag{B3}$$

and to the photoelectric $B_J$ system by

$$B_J=J+0.1 \tag{B4}$$

(Shanks *et al.* 1984; Ellis 1983). Thus, for a disc with $(B-V)\approx(J-F)_{KOS}=0.7$ we infer

$$B_J\approx J_{KOS}-0.7 \tag{B5}$$

which is in reasonable agreement with the empirical transform $B_J=J_{KOS}-0.64$ deduced in Paper III.